The Hepatic Integrated Stress Response Suppresses the Somatotroph Axis to Control Liver Damage in Nonalcoholic Fatty Liver Disease

By

Wei-Chieh Mu

A dissertation submitted in partial satisfaction of the

requirements for the degree of

Doctor of Philosophy

In

Endocrinology

in the

Graduate Division

of the

University of California, Berkeley

Committee in charge:

Professor Gary Firestone, Chair
Professor Peter Sudmant
Professor Polina Lishko

Spring 2023

Abstract

The Hepatic Integrated Stress Response Suppresses the Somatotroph Axis to Control Liver Damage in Nonalcoholic Fatty Liver Disease

By

Wei-Chieh Mu

Doctor of Philosophy in Endocrinology

University of California, Berkeley

Professor Gary Firestone, Chair

Nonalcoholic Fatty Liver Disease (NAFLD) is a progressive liver disease that can lead to liver cirrhosis and hepatocellular carcinoma, eventually resulting in death. The disease is prevalent worldwide, affecting around a quarter of the population, and is associated with risk factors such as obesity and type 2 diabetes. Currently, no standard treatment exists for NAFLD, which is characterized by excessive hepatic lipid accumulation leading to ER and mitochondrial stress, impaired insulin signaling, and inflammatory response. These events form a vicious cycle and exacerbate the progression of NAFLD. Sirtuin 7 (SIRT7), an NAD^+-dependent deacetylase, is a nutrient sensor that alleviates ER stress and mitochondrial protein folding stress and prevents fatty liver. The insulin/IGF-1 signaling is the first nutrient-sensing pathway reported to regulate longevity in model organisms. Inhibiting the Insulin/IGF-1 signaling extends the lifespan of mice and worms. Paradoxically, low circulating IGF-1 is linked to hepatic steatosis and severe liver fibrosis in NAFLD. It remains unclear whether the somatotroph axis, which controls the insulin/IGF-1 signaling pathway, plays a role in liver damage during the progression of NAFLD.

This dissertation aimed to explore the underlying mechanisms of NAFLD and develop a novel therapeutic strategy to combat this progressive liver disease. Chapter 1 provided a comprehensive review of the current state of nutrient-sensing pathways and oxidative stress response. We also discussed the therapeutic opportunities to prevent aging- or disease-driven tissue dysfunction by targeting the nutrient-sensing pathways. In Chapter 2, we investigated the role of the somatotroph axis in NAFLD and identified a novel regulatory pathway involving hepatic ER stress and ATF3, which suppresses the somatotroph axis in hepatocytes and leads to decreased cell proliferation and ER stress-induced cell death. Our findings in genetic and diet-induced NAFLD mouse models suggest that the suppressed somatotroph axis prevents apoptosis and inflammation but decreases hepatocyte proliferation and exacerbates fibrosis in the livers. Finally, we demonstrated that pharmacological activation of SIRT7 via NAD^+ boosting reduces hepatic ER stress, rescues the suppressed somatotroph axis, and ameliorates NAFLD pathogenesis, offering a promising new therapeutic approach for treating this disease.

Dedication

This dissertation is dedicated to my parents,

Who have given the unconditional love and support to pursue my dreams.

Table of Contents

List of Figures

Figures for chapter 1

Figures for chapter 2

Acknowledgments

First and foremost, I would like to express my heartfelt gratitude to my advisor, Dr. Danica Chen, for her support and guidance throughout my Ph.D. education. Dr. Chen has been a phenomenal mentor, providing me with invaluable opportunities to work with cutting-edge technologies and contributing significantly to my academic and personal growth. I am deeply grateful for her support, which has been instrumental in enabling me to accomplish what I have during my time as a graduate student. I would also like to thank my dissertation committee, Dr. Peter Sudmant and Dr. Polina Lishko, for their helpful guidance on my research projects.

I am incredibly grateful for the financial support I have received during my Ph.D., including the Government Fellowship for Study Abroad (Taiwan, Ministry of Education), the Dr. and Ms. James C.Y. Soong Fellowship (UC Berkeley), and the Frontier in Medical Research Fellowship (QB3). These fellowships have allowed me to pursue my research goals and have been an invaluable contribution to my academic career.

The work in this dissertation has been published in two papers [1,2], and I would like to acknowledge the contributions of everyone in the Chen lab. I am especially thankful to Hanzhi for teaching me HSC-related experiments, Tony for teaching me co-IP, Rika for being a dear lab sister, Irene and Carolyn for helping with countless genotyping, Chih-Ling for teaching me brain histology, Marine for kindly assisting with the challenging ChIP-seq, and Annie, Yifei, Ayane, Jenny, and Anna for their generous assistance whenever I needed it.

"*A good friend is like a four-leaf clover; hard to find and lucky to have.*" I would like to take a moment to express my gratitude to my best friend, Sneha, for always being there for me. Fortunately, I have found her at Cal and am grateful for our friendship. I would like to thank the sitcoms that have provided me laughter during the ups and downs of graduate school: *Friends*, *The Big Band Theory*, *Parks and Recreation*, and *The Office*. Thank you for making my life more joyful, especially during the COVID-19 pandemic. I am also grateful to all the boba tea shops for providing sweet moments during my graduate school years.

Lastly, I thank my parents for their unwavering love, support, and encouragement throughout my journey. Their sacrifices, dedication, and belief in me have been instrumental in enabling me to pursue my dreams. Thank you for indulging me in going to a foreign land that's 7000 miles away and spending all these years on getting this degree.

With my degree now completed, I am excited and ready to embark on the next chapter of my life.

Chapter 1: Nutrient sensing, the oxidative stress response, and stem cell aging

Abstract

The free radical theory of aging was first proposed by Harman in the 1950s with the idea that oxidative damage accumulates with age and contributes to functional deteriorations during aging. Caloric restriction (CR) has been shown to be one of the most effective approaches to extend life span and health span. Recent advances in nutrient sensing have identified molecular regulators responsible for CR-mediated oxidative stress defense and underscore their importance in preserving stem cell maintenance and tissue integrity during aging. Deciphering molecular mechanisms of the oxidative stress response during CR will enhance our knowledge toward the biology of aging and provide insights into developing activators targeting the nutrient-sensing pathways to extend healthspan and lifespan.

Introduction

Nutritional intervention is an effective approach to extend lifespan and ameliorate age-associated dysfunctions. In 1935, McCay published the first piece of evidence that reduced food intake extends the lifespan of rodents [3]. Since then, this dietary regimen has been studied extensively in different model organisms [3-6]. CR, which usually refers to a 20% to 50% reduction of total energy intake without malnutrition [7], is considered to be the most consistent and effective intervention to prolong lifespan across species including yeast, worms, rodents and perhaps non-human primates [3-6]. In mammals, CR has been shown to induce a wide spectrum of health benefits and ameliorate the development of age-related diseases including cancer, immunological disorders, and neurodegenerative diseases [8-10]. Besides restriction of calories, other nutrition restrictions, such as glucose restriction, methionine restriction, and protein restriction, also have profound effects on lifespan and healthspan [11-13], and sparked a widespread interest in understanding how nutrition restriction works.

Proposed by Denham Harman in the 1950s, the free radical theory of aging postulated that aging and age-related degenerative diseases are attributed to the attacks of reactive oxygen species (ROS) on cell components such as lipids, DNA, and proteins [14-16]. Since then, numerous studies have shown that ROS levels increase during aging [17-19]. Coincidently, oxidative damage to lipids, DNA, and proteins accumulates in various animal models with age [20]. Despite the surprising finding that genetic activation of a number of antioxidant enzymes did not extend the lifespan of mice [21], mounting evidence supporting a causal relationship between oxidative stress and aging continues to emerge [21-26] and reestablishes oxidative stress as the focal point of aging research. Oxidative stress under normal physiological condition is considered oxidative eustress, when ROS act as signaling molecules to regulate cell proliferation, migration, and adaptive stress

responses [27,28]. When intracellular concentrations of ROS are above the normal range, oxidative distress triggers inflammation, cell growth arrest, and cell death.

Among various nutrition restrictions, CR has been studied most extensively. It was proposed that CR slows aging by reducing the metabolic rate and therefore preventing the production of ROS [29]. However, recent advances in nutrient sensing challenged this traditional view and support the notion that CR triggers active oxidative stress responses elicited by nutrient sensors to reduce cellular oxidative damage and the mitochondrial deterioration, and that this regulatory network is particularly important in preserving adult stem cell maintenance and tissue homeostasis during the aging process. Deciphering the molecular mechanisms of the oxidative stress response during CR will enhance our knowledge toward the biology of aging and provide insights into therapeutic development to prevent or reverse aging-associated tissue degenerative conditions and diseases.

Nutrient Sensing and the Oxidative Stress Response

The most compelling evidence supporting an active oxidative stress response during CR came from the studies of SIRT3. SIRT3 belongs to the sirtuin family of NAD^+-dependent deacylases and it is localized in the mitochondrial matrix [30,31]. Mice lacking SIRT3 are phenotypically normal at a young age and exhibit no difference in oxidative damage markers compared to wild-type mice when fed *ad libitum* [32]. However, while wild-type mice are protected from oxidative damage when fed a CR diet, SIRT3 KO mice are not [32], providing direct genetic evidence linking SIRT3 to CR-induced protection from oxidative stress. Importantly, SIRT3-mediated protection from oxidative stress is physiologically relevant. While wild-type mice fed a CR diet are protected from hearing loss, a well-establish oxidative stress-related pathology, SIRT3 deficient mice lose such a protection [33] (Figure 1).

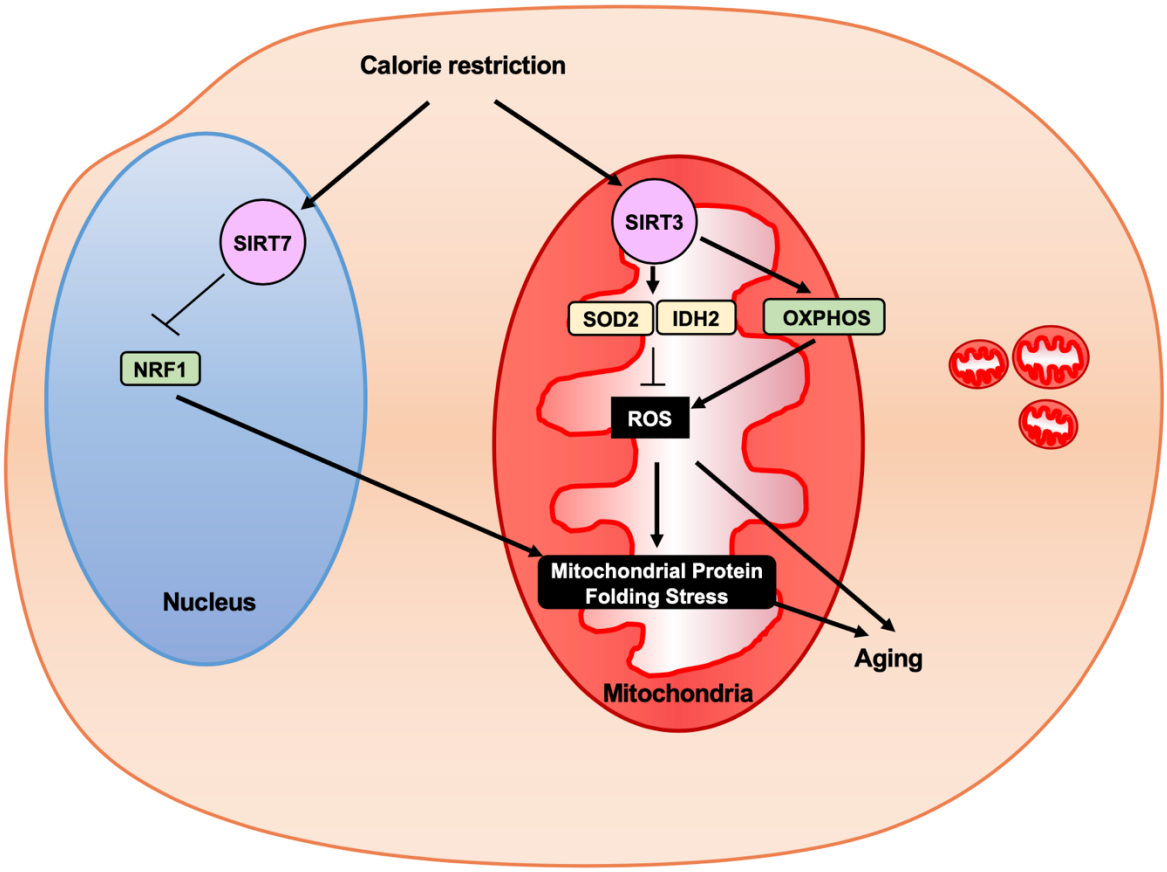

Figure 1. Caloric restriction induces nutrient sensors SIRT3 and SIRT7 to actively reduce oxidative stress and damage.

During caloric restriction, cells undergo a metabolic switch from glycolysis to oxidative phosphorylation for efficient energy production. Caloric restriction induces SIRT3, which activates SOD2 and IDH2 via deacetylation to scavenge ROS, a byproduct of respiration. SIRT7 represses NRF1 and mitochondrial translation to alleviate mitochondrial protein folding stress induced by ROS. Together, SIRT3 and SIRT7 alleviate the mitochondrial oxidative stress and mitochondrial protein folding stress during caloric restriction. The enhanced stress resistance provides protection against age-related degeneration. OXPHOS: oxidative phosphorylation, SIRT3: sirtuin 3, SIRT7: sirtuin 7, IDH2: isocitrate dehydrogenase 2, SOD2: superoxide dismutase 2, NRF1: nuclear respiratory factory 1.

Mounting evidence has demonstrated that SIRT3 plays a universal role in ameliorating oxidative stress in various cell types. SIRT3 is needed to prevent oxidative stress and injury in hepatocytes, myoblasts, pancreatic beta cells, cardiomyocytes, mouse embryos, proximal tubular cells, neural stem cells, dopaminergic neurons, fibroblasts, and osteoblasts [34-44]. SIRT3 also protects endothelial cells and oocytes from diet-induced oxidative stress [45-47].

At the organismal level, SIRT3 deficient mice at an older age develop exacerbated oxidative stress-related physiological defects including diet-induced obesity, insulin resistance, hyperlipidemia, steatohepatitis, intracerebral hemorrhage, tumor formation, inflammation, sarcopenia, and reduced hematopoietic stem cell count and function [38,39,48-57]. Consistently, SIRT3 activity is inversely correlated with energy intake. SIRT3 mRNA and protein levels are increased by fasting or CR in mouse skeletal muscle, liver, and brown adipose tissue [39,51,58,59], whereas its expression is decreased by overnutrition [57]. These studies suggest that SIRT3 is upregulated during CR and triggers a protective program to reduce oxidative stress and damage, contributing significantly to the wide spectrum of beneficial effects of this dietary regimen.

Mechanistically, SIRT3 is the primary deacetylase located in the mitochondria. One critical downstream event that mediates SIRT3-induced reduction of oxidative stress is the activation of superoxide dismutase 2 (SOD2), a key antioxidant in the mitochondria that catalyzes the first step of superoxide detoxification [32,60]. SOD2 is modified post-translationally via acetylation in cells and is a bona fide substrate of SIRT3 [32,60]. By targeting the lysine residues adjacent to the catalytic center of SOD2 for deacetylation, SIRT3 promotes the enzymatic activity of SOD2 [32]. Conceivably, these two lysine residues, when exposed, increase the positive charge around the active site and improve the efficiency of trapping the negatively charged superoxide. SOD2 activity is induced via SIRT3-mediated deacetylation during CR as SIRT3 KO mice have higher acetylated SOD2 and lower enzymatic activity compared to the wild-type mice during CR but not when fed *ad libitum* [32] (Figure 1).

Another SIRT3 substrate that accounts for its function to dampen oxidative stress is isocitrate dehydrogenase 2 (IDH2), an $NADP^+$-dependent mitochondrial enzyme that controls the mitochondrial redox balance by generating the reducing agent NADPH [61]. NADPH is used by glutathione reductase to regenerate glutathione (GSH) from its oxidized form glutathione disulfide (GSSG) [61]. GSH can then be used by glutathione peroxidase to reduce hydrogen peroxide [62,63]. SIRT3 directly deacetylates and activates IDH2 during CR in multiple tissues, resulting in increased oxidative stress resistance by enhancing NADPH levels and the ratio of reduced-to-oxidized glutathione (GSH: GSSG) [33]. These findings provide the molecular evidence that SIRT3 acts as a nutrient sensor that is turned on during CR to activate mitochondrial antioxidant defense system and alleviate oxidative stress and damage (Figure 1).

Interestingly, proteomic studies identified a large number of non-histone proteins that are modified post-translationally by acetylation, including roughly 30% of mitochondrial proteins [64-66]. SIRT3 regulates the global acetylation landscape of mitochondrial proteins, many of which catalyze the rate-limiting steps of the metabolic pathways, and initiates a metabolic reprogramming toward activated metabolic flux in the mitochondria [54]. This metabolic reprogramming allows animals to switch from glycolysis to fatty acid oxidation. This metabolic switch is essential for the survival of the CR animals, which have reduced levels of blood glucose, and prevents the development of hypoglycemia and death. This metabolic switch is also advantageous for animals experiencing limited food supplies, as switching from energy-inefficient glycolysis to energy-efficient oxidative phosphorylation allows the animals to produce the most energy out of the limited food supply. However, this metabolic switch comes at a cost, which is the production of ROS, a natural byproduct of cellular respiration. The activation of the mitochondrial antioxidative system concomitant with this metabolic switch is viewed as an evolved adaptation to cope with the increased production of ROS. The net effect is enhanced oxidative stress resistance and improved protection of the cells and the organisms.

Human clinical studies have shed light on the potential to manipulate SIRT3 activity by CR and alleviate oxidative damage. 24-hr fasting in healthy individuals leads to the deacetylation and activation of SOD2, lower ROS levels, and less production of proinflammatory interleukin-1β in the peripheral blood mononuclear cells [55]. 3 weeks of intermittent fasting, an alternative dietary regimen to CR achieved by alternating days of fasting (25% of normal caloric intake) and feasting (175% of normal), in healthy individuals leads to a trend of increase in SIRT3 expression ($p = 0.0772$) in the peripheral blood mononuclear cells [67]. More studies are needed to demonstrate the safety, feasibility, and effectiveness of different dietary regimens on alleviating oxidative stress and oxidative stress-related disease progression in humans.

Nutrient Sensing and the Mitochondrial Protein Folding Stress Response

The essence of the free radical theory of aging is that ROS generated as natural byproducts of cellular respiration cause damage to the molecular components inside the mitochondria due to proximity, unleashing a vicious cycle of defective electron transport chain and increased production of ROS [68]. Thus, in addition to enhance the detoxification of ROS produced upon the metabolic switch during CR, it is equally important to enhance the repair of the damage to the molecular components inside the mitochondria. ROS cause protein damage [28,69] and the resulting protein folding stress in the mitochondria is alleviated by inducing the mitochondrial unfolded protein response (UPR), a retrograde signaling cascade from the mitochondria to the nucleus that induces the production of nucleus-encoded mitochondrial proteases and chaperones [70,71].

SIRT7, a sirtuin family member in the nucleus and a histone deacetylase, was recently discovered to regulate a novel branch of the mitochondrial UPR [72]. SIRT7 expression is induced upon mitochondrial protein folding stress and is recruited to the promoters of mitochondrial ribosomal proteins through its interaction with the transcription factor nuclear respiratory factory 1 (NRF1) to repress their gene expression. This leads to

reduced translation, limiting the amount of proteins produced and transported into the mitochondria and alleviating the protein folding burden in this organelle. Lack of SIRT7 leads to constitutive mitochondrial protein folding stress and SIRT7-deficient cells are prone to cell death induced by mitochondrial protein folding stress [72] (Figure 1). At the organismal level, SIRT7 deficient mice develop fatty liver, hearing loss, heart failure, adipose tissue dystrophy, exercise intolerance, and hematopoietic stem cell aging, at least in part due to mitochondrial stress [72-75].

Similar to SIRT3, SIRT7 also appears to play a role in nutrient sensing and its expression fluctuates under different nutrient status. It is increased by glucose deprivation and decreased upon overnutrition [72,76]. Another layer of nutrient sensing by SIRT7 is at the level of post-translational modification. SIRT7 is methylated at arginine 388 and its enzymatic activity is reduced under high glucose conditions, and this modification and its activity are reversible under low glucose conditions [77]. Fittingly, SIRT7 overexpression improves the survival of glucose-starved cells, whereas SIRT7 knockdown reduces the survival of glucose-starved cells partly mediated through NRF1, indicating that SIRT7 promotes the survival of glucose starved cells at least in part by its protection of the mitochondrial stress [72].

Oxidative Stress, Stem Cell Aging, and Tissue Degeneration

The beneficial effects of mitochondrial oxidative stress resistance in metabolic tissues have been reviewed extensively. Here, we are focusing on the recent studies on adult stem cells, which persist throughout the lifespan to maintain and repair tissues. Stem-cell exhaustion is one hallmark of aging, which describes a decline in regenerative capacity of stem cells, contributing to the tissue degeneration and dysfunction during the aging process [78,79]. Intriguingly, CR improves the maintenance of stem cells across tissues [80-84].

Stem cells in the hematopoietic system are among the best studied for their maintenance and deterioration during aging. Most of the adult hematopoietic stem cells (HSCs) remain in a quiescent state with low metabolic rate and mitochondria count, and they rely mainly on glycolysis for energy production [85-87]. Indeed, HSCs have low levels of ROS compared to the differentiated progeny [49]. In addition to low ROS production, HSCs are equipped with high capacity of ROS scavenge, as indicated by the enrichment of forkhead box O 3a (FOXO3a) and SIRT3 in HSCs [49,88]. FOXO3a is a transcription factor known as a longevity gene that controls the expression of antioxidant genes such as SOD2 [89]. HSCs have higher nuclear localization of FOXO3a compared to the differentiated progeny, where FOXO3a is mainly located in the cytosol and its transcriptional activity is silenced [88]. As for SIRT3, its expression level is magnitude higher in HSCs than in its differentiated progeny [49]. The metabolic features of quiescent HSCs and a robust antioxidant defense system ensure the maintenance of HSCs and prevents the depletion of the HSCs pool [90]. Elevated ROS levels caused by activation of AKT and TSC-mTOR pathway [91,92], impaired ATM-mediated DNA damage response [93,94], or defective antioxidative defense due to genetic ablations of FOXOs, NRF2, SIRT3, or TXNIP [49,95-98] all lead to loss of HSC quiescence and self-renewal capacity.

As HSCs transition from quiescence to proliferation, the mitochondrial biogenesis occurs and OXPHOS genes are upregulated in HSCs to support the increased energy demands [99]. Mitochondrial biogenesis and the metabolic switch to using OXPHOS lead to increased production of ROS. While long being viewed as a metabolic waste, ROS have been shown to have physiological functions, at least in the context of stem cells. ROS can act as signaling molecules to prime hematopoietic stem and progenitor cells for differentiation [91,100]. Supporting this view, increased ROS production triggers the differentiation of *Drosophila* hematopoietic progenitors, whereas scavenging ROS prevents their precocious differentiation into mature blood cells [100]. On the other hand, ROS levels have been found increased in HSCs during aging and contribute to the functional deterioration of aged HSCs [49,72,93,101]. These findings again support the free radical theory of aging, arguing that age-related oxidative stress can induce differentiation and death of stem cells, and ultimately drives stem cell aging and tissue degeneration.

The canonical mitochondrial UPR genes are also elevated in HSCs during the transition from the quiescent stage to proliferation, indicating increased mitochondrial protein folding stress caused by mitochondrial biogenesis and ROS production [99]. The mitochondrial UPR is induced to ensure the mitochondrial integrity upon HSC activation. SIRT7 plays an indispensable role in this transition to suppress mitochondrial protein folding stress [72]. Dysregulation of the UPR^{mt} resulting from SIRT7 deficiency leads to the loss of HSC quiescence and impaired regenerative capacity [72], suggesting that SIRT7 ensures the surveillance of mitochondrial protein folding stress in HSCs and prevents stress-induced cell death.

These observations are consistent with a model that the transition of HSCs from quiescence to proliferation is regulated by a mitochondrial metabolic checkpoint to examine the health of the mitochondria at the restriction point before progressing into the cell cycle [72,90,99]. Mitochondrial biogenesis is accompanied by increased mitochondrial oxidative stress and protein folding stress, which are surveilled by SIRT3 and SIRT7 respectively to reduce stress and return to quiescence until the damage is fixed. Failure of the surveillance system results in HSC death and the depletion of the HSC pool. Interestingly, the expression levels of SIRT3 and SIRT7 in HSCs decrease during aging, which correlate with increased cellular ROS and mitochondrial protein folding stress in aged HSCs [49,72]. Overexpression of SIRT3 or SIRT7 in aged HSCs alleviates mitochondrial oxidative stress or mitochondrial protein folding stress, and increases the functional capacity of aged HSCs [49,72], indicating that dysregulation of the mitochondrial metabolic checkpoint underlies the functional deterioration of aged HSCs (Figure 2).

The mitochondrial metabolic checkpoint model of HSC maintenance raises a question of how mitochondrial stress leads to the demise of HSCs. A potential clue came from a recent finding that the NLRP3 inflammasome is a regulator of HSC aging [102]. The NLRP3 inflammasome is an innate immune sensor that is highly expressed in macrophages and can be activated by multiple endogenous damage-associated molecular patterns such as ROS, leading to the activation of its downstream effector, caspase 1, and the secretion of pro-inflammatory cytokines and pyroptosis, a caspase 1-dependent programmed cell death [103-105]. NLRP3 was found to be expressed in HSCs, albeit to a much lower level than in macrophages [102]. Aged HSCs have aberrant activation of the NLRP3

inflammasome compared to young HSCs, and silencing NLRP3 or caspase 1 improves the function of aged HSCs [102]. Alleviating mitochondrial stress by overexpressing SIRT3 or SIRT7 reduces the caspase 1 activity in aged HSCs, while HSCs from mice lacking SIRT7 display increased caspase 1 activation [102]. This study indicates that the NLRP3 inflammasome relays the signal of mitochondrial stress to mediate HSC death.

SIRT2, a sirtuin family member in the cytosol, appears to be a critical regulator of the NLRP3 inflammasome [102,106]. SIRT2 deficient mice display age-dependent defects in HSCs [102]. While SIRT2 KO mice are largely normal in HSCs at a young age, they have reduced HSC maintenance and functional capacity due to aberrant activation of the NLRP3 inflammasome [102]. SIRT2 expression is also reduced in aged HSCs and its overexpression improved the functional capacity of aged HSCs, adding another nutrient sensor regulating the mitochondrial metabolic checkpoint of HSC maintenance and aging [102] (Figure 2).

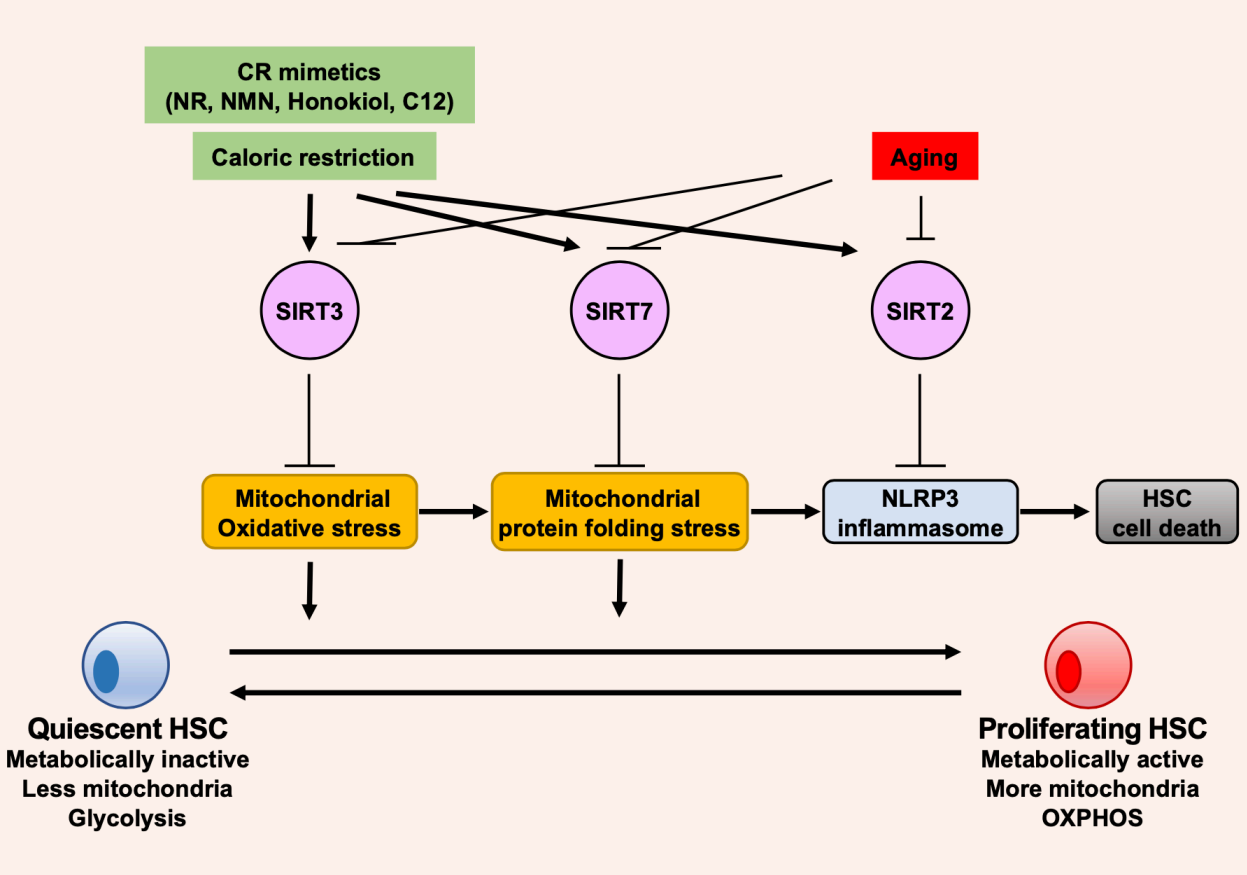

Figure 2. A mitochondrial metabolic checkpoint controls hematopoietic stem cell quiescence and aging.

The transition of quiescent HSCs to proliferation involves mitochondrial biogenesis and elevated mitochondrial oxidative stress and protein folding stress. The mitochondrial stresses are surveilled by SIRT3 and SIRT7 for HSC maintenance. SIRT3 and SIRT7 levels decline with age, which correlates with increased mitochondrial stress in old HSCs. Age-associated mitochondrial stress activates the NLRP3 inflammasome and leads to HSC death. SIRT2 represses the activation of the NLRP3 inflammasome and preserves HSC maintenance. Together, SIRT2, SIRT3, and SIRT7 regulate the mitochondrial metabolic checkpoint that determines the fate of HSCs to either stay quiescent, proliferate, or undergo cell death. CR: caloric restriction, NR: Nicotinamide riboside, NMN: nicotinamide mononucleotide, C12: 7-hydroxy-3-(4′-methoxyphenyl) coumarin, HSC: hematopoietic stem cell, SIRT2: sirtuin 2, SIRT3: sirtuin 3, SIRT7: sirtuin 7.

The mitochondrial metabolic checkpoint, originally discovered in HSCs, also operates in stem cells of other tissue origins. Similar to HSCs, while low levels of ROS are required to stimulate the proliferation of other somatic stem cells such as neural stem cells (NSCs) [107-110] and intestinal stem cells [111], high levels of ROS result in stem cell death. SIRT3 protects NSCs from oxidative stress and apoptosis [40] and disrupting FOXOs causes premature differentiation of NSCs, decreases their self-renewal capacity and eventually leads to the depletion of NSCs [107,108]. ROS also regulate aging of mesenchymal stem cells, and aged human mesenchymal stem cells have weakened antioxidant defense system indicated by decreased SOD2 activity [112].

Mitochondrial UPR also appears to be a regulatory mechanism of stem cells across tissues. Like aged HSCs, aged muscle stem cells also have impaired mitochondrial functions in TCA cycle and OXPHOS, and the mitochondrial UPR gene expression levels are reduced in old muscle stem cells, suggesting that they have less protection against mitochondrial protein folding stress [113]. Disruption of HSP60, a key chaperone in the mitochondria and a major player of the mitochondrial UPR, leads to compromised intestinal stem cell maintenance and function [114].

Together, these findings raise the possibility that the oxidative stress-induced stem cell aging may be reversed by inducing cellular protective mechanisms. Activating these nutrient sensing pathways via CR or even better CR mimetics may be a useful strategy to enhance oxidative stress resistance, alleviate stem cell aging, and delay or even reverse tissue degeneration during aging.

Therapeutic Opportunities

A large body of evidence supports that CR holds a promise to improve healthspan partly through alleviating oxidative stress. However, this diet is not sustainable by most people. Small-molecule CR mimetics is a tempting alternative to achieve its prolongevity effects through modulating the activities of nutrient sensors. Intriguingly, many nutrient sensors are enzymes and are likely druggable. There are several small molecule activators of sirtuins being reported over the past few years [115]. The intermediates in the NAD^+ biosynthetic pathways are intuitive candidates to serve as sirtuin activators due to their enzymatic dependence on NAD^+. In mammals, NAD^+ can be generated through the salvage pathway from nicotinamide mononucleotide (NMN) by NMN adenylyltransferase (NMNAT) [116]. Nicotinamide riboside (NR), another key NAD^+ precursor, is converted to NMN by nicotinamide riboside kinase [117]. NAD^+ can also be generated through the *de novo* NAD^+ synthetic pathway from tryptophan. In the *de novo* pathway, the intermediate α-amino-β-carboxymuconate-ε-semialdehyde (ACMS) can be converted to α-amino-β-muconate-ε-semialdehyde (AMS) by ACMS decarboxylase (ACMSD) and diverted away from NAD^+ production [118,119].

NAD^+ level decreases with age in metabolic tissues (pancreas, liver, white adipose tissue and skeletal muscle) and hippocampus of mice [120-122]. 6 weeks of CR or 1 week of NMN supplementation elevate NAD^+ in the skeletal muscle of aged mice [123]. NMN also increases NAD^+ levels in the hippocampus and improves the proliferation and

maintenance of NSCs, suggesting it is able to cross the blood-brain barrier [122]. Remarkably, a single dose of NMN is sufficient to reverse the glucose intolerance of aged diabetic mice [120]. Moreover, a recent paper reported that 10-week NMN treatment (250 mg/day) increased insulin sensitivity in the muscle of prediabetic women in a randomized, placebo-controlled, double-blind trial [124]. Pharmacological inhibition of ACMSD, which is mainly expressed in the liver and kidney, boosts the endogenous NAD^+ levels, induces SOD2 activity, and protects mice from diet-induced hepatic steatosis and acute kidney injury [125].

NR increases NAD^+ levels and activates SIRT3, which further leads to the deacetylation and activation of its target SOD2, and reduces ROS levels [55,126,127]. Long-term NR supplementation showed tissue-specific inductions of NAD^+ levels including skeletal muscle, muscle stem cells, liver, and brown adipose tissue, but not in the brain or white adipose tissue [113,126]. NR induces the two mitochondrial stress defense systems, mitochondrial UPR and SOD2 activity [121]. NR supplementation prevents diet-induced obesity in mice by increasing energy expenditure [126], and protects mice from hearing loss through the prevention of neurite retraction from inner hair cells, which is mediated by SIRT3 activity [127].

Consistent with the role of sirtuins in the mitochondrial metabolic checkpoint that prevents stem cell aging and activation of the NLRP3 inflammasome, NR inhibits the activation of the NLRP3 inflammasome in macrophages [55] and prevents stem cell aging. In HSCs, NR represses mitochondrial activity, induces mitochondrial UPR, enhances the engraftment of human hematopoietic progenitor cells, and improves the survival of mice after lethal irradiation and limiting-dose-HSC transplantation [128]. NR delays the senescence of adult muscle stem cells in aged mice by activating the mitochondrial UPR and improving mitochondrial function [113]. NR also improves the function and numbers of neural and melanocyte stem cells [113]. Importantly, NR increases the lifespan of aged mice when supplementation started at 24 months of age [113]. A recent clinical trial suggests that chronic NR supplementation is well-tolerated in healthy middle-aged and older adults, and NR effectively increases NAD^+ levels in peripheral blood mononuclear cells [129]. Replenishing NAD^+ shows promise to serve as CR mimetics and prevent stem cell aging and tissue degeneration through inducing mitochondrial stress resistance and improving mitochondrial function.

Honokiol, a natural biphenolic compound with antioxidative property, increases SIRT3 expression, induces the deacetylation of mitochondrial proteins, and reduces ROS levels in mice and rats [57,130-132]. Honokiol limits ROS production and prevents the cardiac hypertrophic response *in vitro* and *in vivo*, but the protective effects were lost in SIRT3 KO conditions [130]. Additionally, Honokiol prevents high glucose-induced apoptosis and NF-κB activation in human umbilical vein endothelial cells [133]. Honokiol reduces ROS levels in diabetic rats with intracerebral hemorrhage in a SIRT3-dependent manner, and subsequently decreases NLRP3 inflammasome activation [57]. The antioxidant and antidiabetic effects of Honokiol have been studied mainly in animal models [134]. Future studies are needed to evaluate its therapeutic potentials for human diseases.

Another activator of SIRT3, 7-hydroxy-3-(4′-methoxyphenyl) coumarin (C12), has been recently identified to activate SIRT3 and its substrate SOD2 [135]. C12 binds to the NAD^+ pocket of SIRT3 and leads to the deacetylation and activation of SOD2 [135]. C12 reduces mitochondrial superoxide levels in HEK293T cells and primary rat astrocytes in a SIRT3-dependent manner [135]. In the motor neurons generated from amyotrophic lateral sclerosis (ALS) patient-derived induced pluripotent stem cells, C12 promotes their survival and improves neuronal morphology [136]. Metabolically, C12 enhances mitochondrial respiration and complex I activity in ALS patient-derived motor neurons, while reduces glycolysis and mitochondrial ROS levels [136]. These natural-derived small-molecule activators of SIRT3 may be useful CR mimetics and induce the favorable health outcome as CR. The SIRT3 activators need to be tested in a broader range of cell types and disease models but highlight the potentials to serve as treatments for oxidative stress-related disease. It would also be critical to investigate if the time of administration, i.e., later in life, would influence the effectiveness of these SIRT3 activators on reducing oxidative damage and preventing tissue degeneration. Compared to SIRT3, small-molecule activators of SIRT7 and SIRT2 remain to be developed.

Since oxidative stress can trigger the activation of NLRP3 inflammasome, repressing its activation may alleviate the proinflammatory pathologies caused by ROS. MCC950 is a selective small-molecule inhibitor of NLRP3 that abolishes the assembly of NLRP3 inflammasome, hence its activation and the production of proinflammatory cytokine IL-1β [137]. MCC950 inhibits the ROS-induced NLRP3 inflammasome activation in the lung ischemia-reperfusion mouse model and protects mice from lung injury [138]. The inhibitor of NLRP3 inflammasome provides another layer of regulation of oxidative stress-induced damage and prevents tissue degeneration.

Conclusion

Recent advances in the molecular regulation of the oxidative stress response by nutrient sensors provide evidence that energy deprivation activates certain nutrient sensors to trigger the antioxidant defense system and subsequently prevent age-associated degeneration. Future studies of the oxidative stress response induced by CR in different tissues or cell types will elucidate if the response is tissue-specific or ubiquitous. It will also be important to investigate the physiological significance of this protective antioxidant defense mechanism induced by CR, that is, whether the activation of these nutrient sensors slows the aging process or delays the disease progression through reducing oxidative stress and damage. This knowledge will be a solid foundation for designing small molecule activators of these nutrient sensors to target oxidative stress-related diseases.

Chapter 2: The Hepatic Integrated Stress Response Suppresses the Somatotroph Axis to Control Liver Damage in Nonalcoholic Fatty Liver Disease

Abstract

Nonalcoholic fatty liver disease (NAFLD) can be ameliorated by calorie restriction, which leads to the suppressed somatotroph axis. Paradoxically, suppressed somatotroph axis is associated with NAFLD patients, in particular, correlated with the severity of fibrosis. How the somatotroph axis becomes dysregulated and whether the repressed somatotroph axis impacts liver damage during the progression of NAFLD are unknown. Here, we identified a regulatory branch of the hepatic integrated stress response (ISR), which represses the somatotroph axis in hepatocytes through ATF3, resulting in enhanced cell survival and reduced cell proliferation. In mouse models of NAFLD, the ISR represses the somatotroph axis, leading to reduced apoptosis and inflammation but decreased hepatocyte proliferation and exacerbated fibrosis in the livers. NAD^+ repletion reduces the ISR, rescues the dysregulated somatotroph axis, and alleviates NAFLD. These results establish the hepatic ISR suppresses the somatotroph axis to control cell fate decision and liver damage in NAFLD.

Introduction

The current challenges in developing therapeutics against nonalcoholic fatty liver disease (NAFLD) reflect its complex nature, raising the question whether the solution requires a combination of drugs. NAFLD can be ameliorated by calorie restriction, which leads to the suppressed growth hormone/insulin-like growth factor-1 (IGF-1) somatotroph axis, a conserved regulator of lifespan that triggers the activation of cellular protective program and the re-allocation of resources from growth to somatic preservation [139-147]. Paradoxically, suppression of the somatotroph axis is associated with NAFLD patients, in particular, correlated with the severity of fibrosis [148-157]. Whether the somatotroph axis controls liver damage during the progression of NAFLD is unknown.

NAFLD begins with hepatosteatosis and can progress to nonalcoholic steatohepatitis (NASH) in response to ER stress [158-160]. The integrated stress response (ISR) is a critical regulator of protein homeostasis at the cellular and organismal level to control the pathogenesis of complex diseases [161]. Little is known about the connectivity of the ISR to other intracellular signaling networks to determine cell fate decision and physiological output. The growth hormone/IGF-1 somatotroph axis includes the secretion of growth hormone from the somatotropes of the pituitary gland into the circulation and the subsequent stimulation of IGF-1 production, which is synthesized and secreted by the liver [162]. While evidence is emerging that systemic ER stress induction leads to the suppressed somatotroph axis [163], whether hepatic ER stress regulates the somatotroph axis autonomously and the molecular mechanism underlying such regulation remain unexplored.

In this study, we show that hepatic ER stress suppresses the somatotroph axis autonomously through the transcription factor ATF3. We provide evidence that suppression of the somatotroph axis results in reduced apoptosis and inflammation but decreased hepatocyte proliferation and exacerbated fibrosis in the livers, offering explanations for the paradoxical observations that the suppressed somatotroph axis is associated with NAFLD patients while calorie restriction suppresses the somatotroph axis and prevents the development of NAFLD at the early stage. Finally, we demonstrate the therapeutic implication of this regulatory pathway for NAFLD.

Results

A mouse model of NAFLD with the suppressed somatotroph axis

To investigate how ER stress and the ISR drive the progression of liver damage in NASH and avoid the confounding factors derived from the diets that are commonly used to induce NASH, we employed a mouse NASH model deficient in the histone deacetylase SIRT7, which develops spontaneous NASH resembling human fatty liver disease when fed a chow diet due to elevated ER stress [73,74,164]. Single-cell RNA-sequencing of the livers of wild-type and *SIRT7*$^{-/-}$ mice using the 10x Genomics Chromium platform and the pathway analysis of differentially expressed genes showed that NAFLD genes were highly enriched in several cell populations (hepatocytes, macrophages, and plasma B cells) of *SIRT7*$^{-/-}$ livers (Figure 1A-C, Figure S1A-E, Table S1, 2), validating the NAFLD mouse model.

Microarray analysis of the livers of wild-type and *SIRT7*$^{-/-}$ mice showed that a number of genes in the somatotroph growth axis and other mitogenic signals were differentially expressed between these two genotypes. The expression of several pro-growth factors, such as growth hormone receptor (GHR), fibroblast growth factor 1 (FGF1), epidermal growth factor receptor (EGFR), fibroblast growth factor receptor 4 (FGFR4), was suppressed in the livers of *SIRT7*$^{-/-}$ mice (Figure S2). IGF binding proteins that positively correlate with the level of IGF-1, such as IGF binding protein 3 (IGFBP3) and IGF binding protein acid labile (IGFALS), were also suppressed in the livers of *SIRT7*$^{-/-}$ mice, while IGF binding proteins that generally inhibit the activity of IGF-1, such as IGF binding protein 1 (IGFBP1), were upregulated. This pattern of gene expression changes in the livers of *SIRT7*$^{-/-}$ mice and wild-type littermates was confirmed by quantitative real-time PCR (Figure 1D-I). The analysis of the single-cell RNA-sequencing data for the livers of wild-type and SIRT7$^{-/-}$ mice revealed that the expression of the somatotroph gene IGF-1 was reduced in the hepatocytes of *SIRT7*$^{-/-}$ liver (Figure 1J, K).

Circulating IGF-1 levels in *SIRT7*$^{-/-}$ mice were significantly lower than their wild-type counterparts (Figure 1L). Consistent with reduced levels of blood IGF-1, the IGF-1 signaling was decreased in the livers of *SIRT7*$^{-/-}$ mice, as evidenced by reduced phosphorylation of Akt (Figure 1M, N). The downregulation of the growth hormone/IGF-1 somatotroph axis in the livers of SIRT7$^{-/-}$ mice is consistent with their post-natal growth retardation [73,164]. Together, these data indicate suppressed somatotroph axis in *SIRT7*$^{-/-}$ mice. This mouse model was therefore used to investigate how the somatotroph axis

becomes dysregulated in NAFLD and to dissect the role of the somatotroph axis in the progression of NASH.

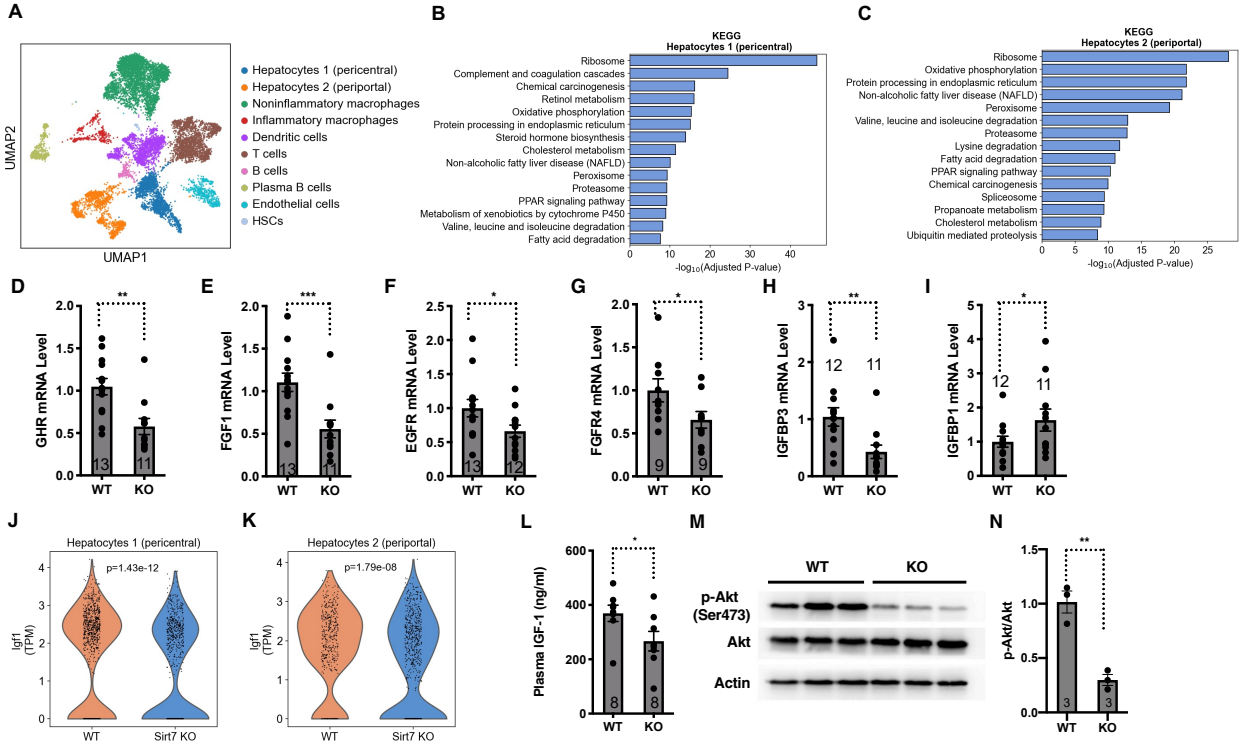

Figure 1. A mouse model of NAFLD with the suppressed somatotroph axis.

(A) Single-cell RNA-sequencing of the livers of WT and *SIRT7*$^{-/-}$ mice using the 10x Genomics Chromium platform. UMAP clustering of single cell transcriptomes (3270 cells from WT and 8340 cells from *SIRT7*$^{-/-}$ mice) colored by cell type. n=3 mice.
(B and C) Pathway analysis for the biological function of differentially expressed genes in hepatocyte 1 (pericentral), and hepatocyte 2 (periportal) of the livers of WT and *SIRT7*$^{-/-}$ mice. n=3 mice.
(D-I) Quantitative real-time PCR analyses for the mRNA levels of the indicated genes in the livers of *SIRT7*$^{-/-}$ mice and wild type controls. GAPDH was used as an internal control. n=9-13 mice.
(J and K) Violin plots comparing log-normalized expression values of IGF-1 in hepatocyte 1 (pericentral) and hepatocyte 2 (periportal) in the livers of WT and *SIRT7*$^{-/-}$ mice. Each dot represents the gene expression levels in one cell. Wilcoxon rank-sum test. n=3 mice.
(L) ELISA quantification of plasma levels of IGF-1 in *SIRT7*$^{-/-}$ mice and wild type controls. n=8 mice.
(M and N) Western analyses (M) and quantification (N) of phosphorylated Akt in the livers of *SIRT7*$^{-/-}$ mice and wild type controls. n=3 mice.
Error bars represent standard errors. * $p < 0.05$; ** $p < 0.01$; *** $p < 0.001$.
See also Figure S1 and S2.

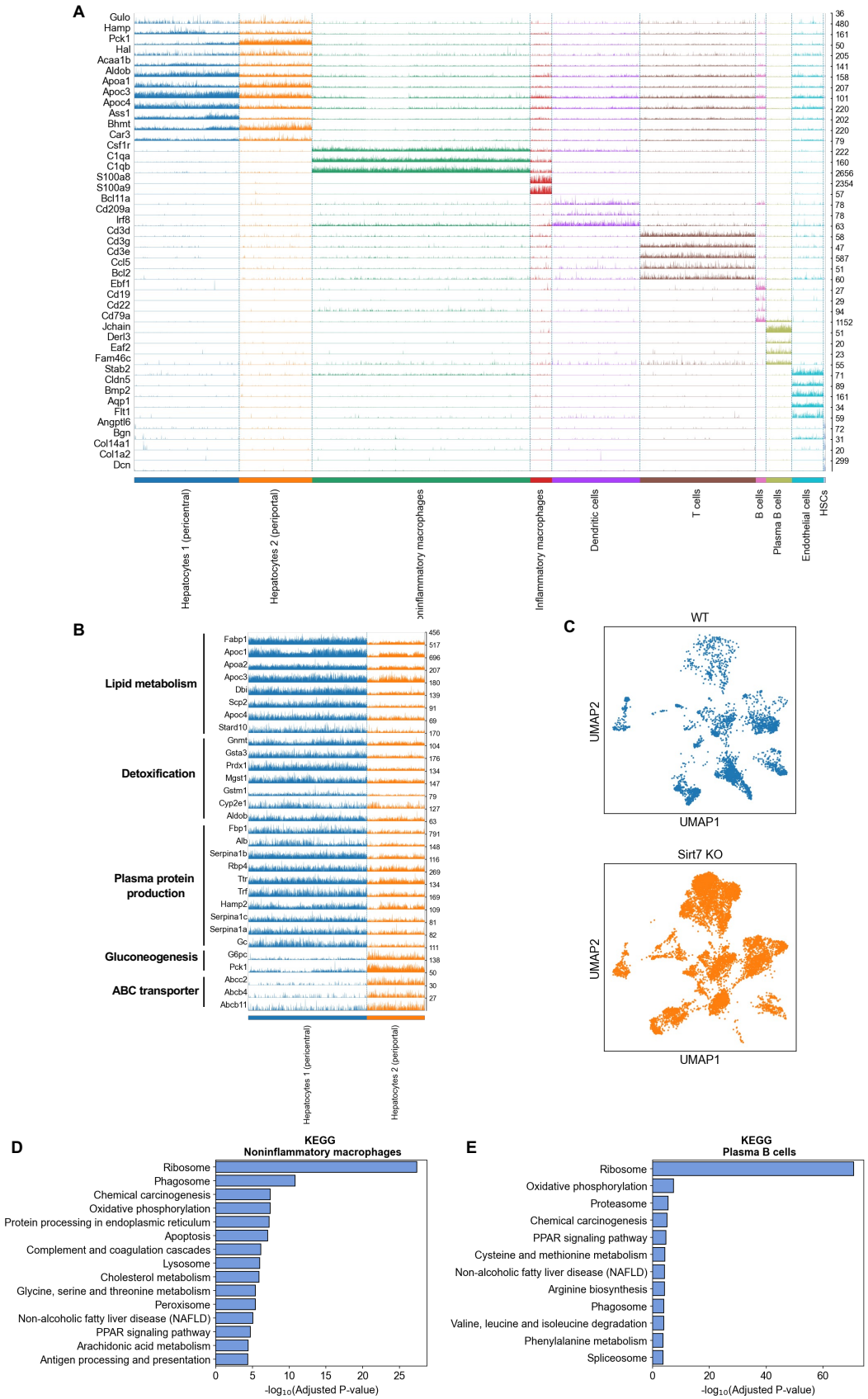

Figure S1. A mouse model of NAFLD.

Related to Figure 1.
(A and B) Quality control for 10x Genomics single-cell RNA-sequencing data of the livers of wild-type and *SIRT7*$^{-/-}$ mice. Track plot showing the expression of representative marker genes for each cell cluster. Each bar represents a cell and cells are grouped based on clustering. The cell identity assigned to each cluster is indicated at the bottom. Numbers on the right indicate maximum detected expression. The gene expression is represented by height (y values). Pericentral hepatocytes express highly genes for lipid metabolism, detoxification, and plasma protein production while periportal hepatocytes express highly genes for gluconeogenesis and ABC transporter.
(C) Single-cell RNA-sequencing of the livers of WT and *SIRT7*$^{-/-}$ mice using the 10x Genomics Chromium platform. UMAP clustering of single cell transcriptomes (3270 cells from WT and 8340 cells from *SIRT7*$^{-/-}$ mice) colored by genotype. n=3 mice. Refer to Figure 1A for cell identity of each cluster.
(D and E) Pathway analysis for the biological function of differentially expressed genes in noninflammatory macrophages and plasma B cells of the livers of WT and *SIRT7*$^{-/-}$ mice.

Gene Title	Gene Symbol	Fold Change	p Value
Growth Hormone Receptor	Ghr	-1.3	0.0019
Fibroblast Growth Factor 1	Fgf1	-1.58	0.0018
Epidermal Growth Factor Receptor	Egfr	-1.39	0.02
Fibroblast Growth Factor Receptor 4	Fgfr4	-1.87	4.16E-06
Prolactin Receptor	Prlr	-2.64	0.0009
IGF Binding Protein, Acid Labile	Igfals	-1.64	0.0003
IGF Binding Protein 3	Igfbp3	-2.16	0.04
IGF Binding Protein 1	Igfbp1	3.74	0.0048
IGF Binding Protein 7	Igfbp7	1.28	0.005
IGF Binding Protein 6	Igfbp6	1.19	0.04

Figure S2. Suppressed somatotroph gene expression in the livers of *SIRT7*$^{-/-}$ mice.

Related to Figure 1.
A summary of genes in the somatotroph axis and mitogenic signaling that are differentially expressed in the livers of *SIRT7*$^{-/-}$ mice compare to the wild type controls based on the microarray analyses. The listed p values are not corrected for multiple testing.

Hepatic ER stress suppresses the somatotroph axis autonomously

SIRT7 deficiency results in constitutive hepatic ER stress [73]. We asked whether suppression of the somatotroph axis in *SIRT7*$^{-/-}$ mice could result from hepatic ER stress and the induction of the ISR autonomously. SIRT7 suppresses ER stress by repressing the activity of the transcription factor Myc and reducing the expression of translation machinery [73]. Consistently, the analysis of the single-cell RNA-sequencing data for the livers of wild-type and *SIRT7*$^{-/-}$ mice showed that ribosome genes were among the most significant changes in various cell types of the liver associated with SIRT7 expression (Figure 1B, C, Figure S1D, E). We knocked down the expression of Myc in the livers of *SIRT7*$^{-/-}$ mice via adenoassociated virus 8 (AAV8)-mediated gene transfer. Myc inactivation repressed the ISR in the livers of *SIRT7*$^{-/-}$ mice, as evidenced by the levels of phosphorylation of eIF2α (Figure 2A, B). Myc inactivation also rescued the expression of genes in the somatotroph axis that were dysregulated in the livers of *SIRT7*$^{-/-}$ mice (Figure 2C-G), increased the plasma levels of IGF-1 (Figure 2H), and enhanced the hepatic IGF-1 signaling (Figure 2I, J), consistent with the suppression of the somatotroph axis by the hepatic ISR autonomously. Furthermore, treatment of hepatocytes with ER stress inducers thapsigargin or tunicamycin resulted in reduced expression of genes in the somatotroph axis (Figure S3A-E). Together, these data suggest that hepatic ER stress and the ISR induction are sufficient to trigger the response in the somatotroph axis autonomously.

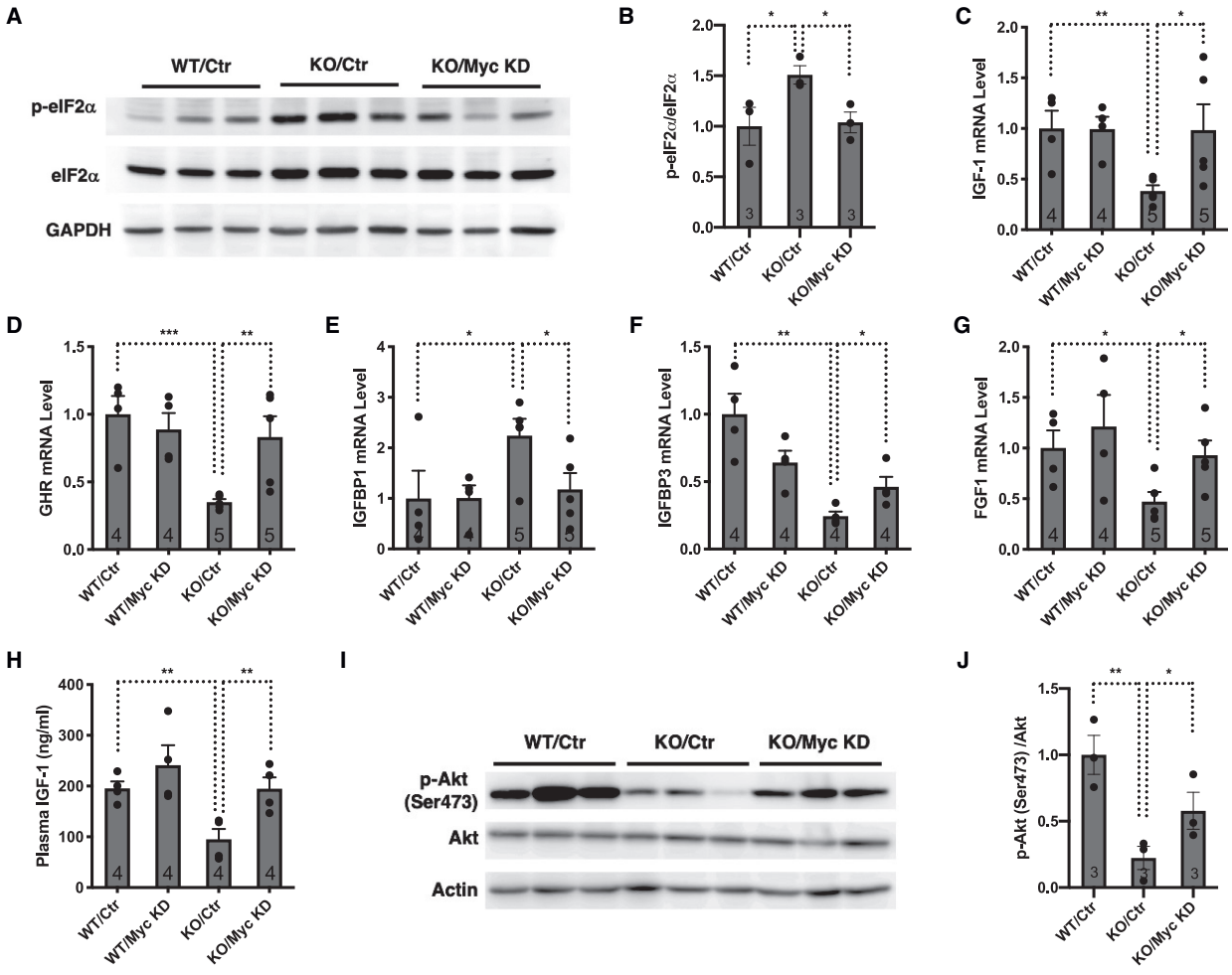

Figure 2. Hepatic ER stress suppresses the somatotroph axis autonomously.

Comparison of wild type and *SIRT7*$^{-/-}$ mice with or without Myc knockdown mediated by AAV8-mediated gene delivery. Mice were analyzed 4 weeks after viral infection.

(A and B) Western analyses (A) and quantification (B) for phosphorylated eIF2α in the livers. n=3 mice.

(C-G) Quantitative real-time PCR analyses for the mRNA levels of the indicated genes in the livers. GAPDH was used as an internal control. n=4-5 mice.

H, ELISA analyses of plasma levels of IGF-1. n=4 mice.

(I and J) Western analyses (I) and quantification (J) for phosphorylated Akt in the livers. n=3 mice.

Error bars represent standard errors. * $p < 0.05$; ** $p < 0.01$.

See also Figure S3.

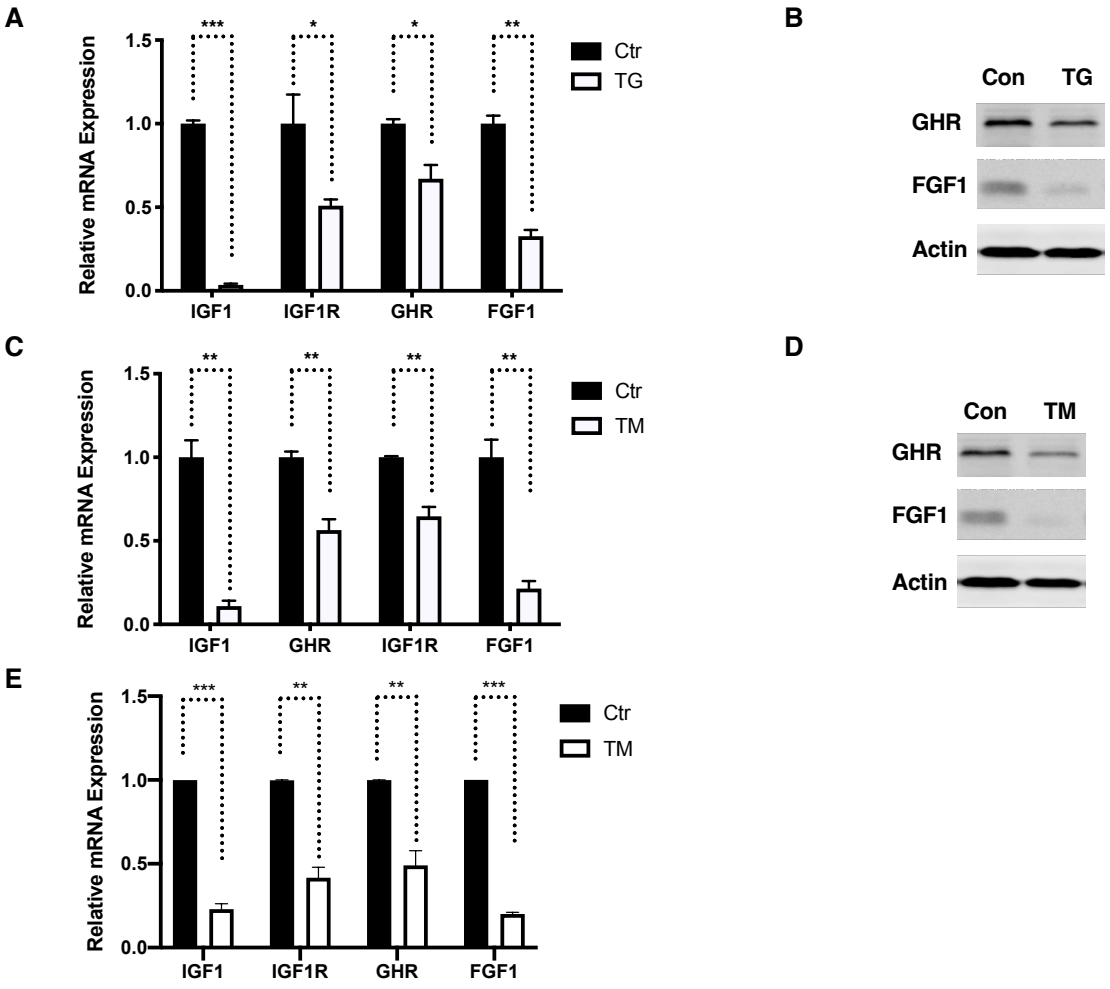

Figure S3. ER stress triggers the suppression of the somatotroph axis in hepatocytes.

Related to Figure 2.
(A-D) Quantitative real-time PCR and Western analyses of expression of indicated genes in Hepa 1-6 cells treated with thapsigargin (A, B) or tunicamycin (C, D). n=2.
E, Quantitative real-time PCR analyses of expression of indicated genes in primary hepatocytes treated with tunicamycin. n=2.
Error bars represent standard errors. * $p < 0.05$; ** $p < 0.01$. ***; $p < 0.001$.

Hepatic ER stress and the ISR suppress the somatotroph axis by inducing ATF3

We next investigated how the hepatic ISR leads to the suppression of the somatotroph axis. ER stress elicits signaling transduction and stress response that allow the cells to restore protein homeostasis [165]. Central to the ISR is the actions of the transcription factors ATF4 and ATF6. ATF3 is also induced by ER stress by a mechanism requiring eIF2 kinases and ATF4, although its role in stress response is obscure ((Figure S4A, B) and [166]). We used the Harmonizome web portal, which is a collection of processed datasets to mine information related to genes and proteins [167], to determine whether the ER stress-related transcription factors could regulate genes in the somatotroph axis. Chromatin immunoprecipitation (ChIP) sequencing data analyses revealed that ATF3 bound to the promotors or enhancers of a number of IGF-related genes (Figure S4C) and ATF4 or ATF6 did not. The binding of ATF3 to the promoters of IGF-related genes was further confirmed by ChIP with an ATF3 antibody followed by quantitative real time PCR in parental hepatocytes (Figure 3A-C) and mouse livers (Figure S4D-F), and was abrogated in ATF3 knockdown (KD) cells generated using two independent short hairpin RNAs (Figure 3D-F). While treatment with the ER stress inducer tunicamycin reduced the expression of genes in the somatotroph axis, ATF3 inactivation blunted the effect (Figure 3G), suggesting that ER stress and the ISR induction repress the somatotroph axis in hepatocytes by inducing ATF3.

Suppression of the somatotroph axis leads to metabolic changes that shift energy usage from growth and proliferation to cellular protection in order to enhance stress resistance, a phenomenon termed hormesis [139,141-146]. ATF3-mediated suppression of the somatotroph axis in response to ER stress and the ISR induction suggests that this branch of the ISR might prevent cell growth and proliferation while activating cellular protective programs and preventing cell death. ATF3 knockdown hepatocytes proliferated faster than control cells (Figure 3H) and exhibited increased apoptosis upon treatment with tunicamycin compared to control cells (Figure 3I). Together, these data suggest that ER stress and the ISR induce ATF3 to repress the somatotroph axis, resulting in reduced proliferation and improved survival of hepatocytes.

ATF3 is a member of the CREB family of basic leucine zipper transcription factors and functions both as a transcriptional activator or repressor [168]. ATF3 is induced in the livers of a rat model of severe steatosis and human NAFLD patients, correlative with the ER stress status [169]. ATF3 was also induced in the livers of *SIRT7*$^{-/-}$ mice (Figure 3J, Table S3). Myc inactivation in the livers of *SIRT7*$^{-/-}$ mice via AAV8-mediated gene transfer suppressed the ISR (Figure 2A, B) and rescued the increased ATF3 expression (Figure 3J), consistent with the induction of ATF3 expression upon the hepatic ISR. To determine whether hepatic ISR results in suppression of the somatotroph axis due to the induction of ATF3, we knocked down the expression of ATF3 in the livers of *SIRT7*$^{-/-}$ mice via AAV8-mediated gene transfer (Figure 3K). ATF3 inactivation in the livers of *SIRT7*$^{-/-}$ mice rescued the dysregulated gene expression of the somatotroph axis (Figure 3L, M), in keeping with the binding of ATF3 to the promoters of IGF-related genes (Figure 3A-C, S4C-F). ATF3 inactivation in the livers of *SIRT7*$^{-/-}$ mice also increased the plasma levels

of IGF-1 (Figure 3N) and the IGF-1 signaling (Figure 3O, P). Together, these data suggest that ATF3 mediates the hepatic ISR-induced repression of the somatotroph axis *in vivo*.

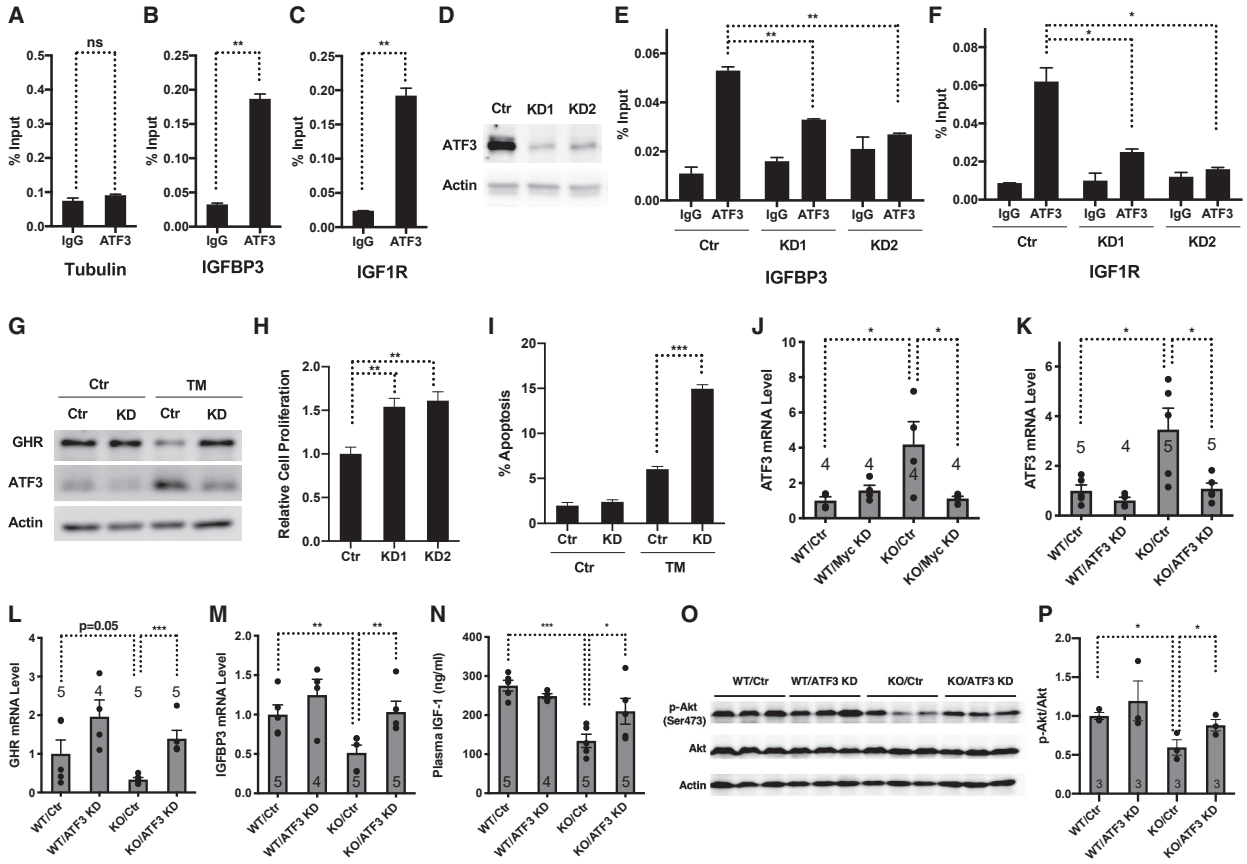

Figure 3. Hepatic ER stress and the ISR suppress the somatotroph axis by inducing ATF3.

(A-C) ChIP with ATF3 antibody followed by quantitative real-time PCR showing ATF3 occupancy at the gene promoters of IGFBP3 and IGF1R in Hepa 1-6 cells. Tubulin was used as a negative control. n = 2.
(D) Western blots showing ATF3 expression in stable ATF3 knockdown Hepa 1-6 cells using shRNA.
(E and F) ChIP with ATF3 antibody followed by quantitative real-time PCR showing reduced ATF3 occupancy at the gene promoters of IGFBP3 and IGF1R in ATF3 knockdown Hepa 1-6 cells. n = 2.
(G) Western analyses of GHR and ATF3 in control and ATF3 knockdown Hepa 1-6 cells with or without tunicamycin induction.
(H) Proliferation of stable ATF3 knockdown Hepa 1-6 cells and control cells. n = 3.
(I) Annexin V staining of ATF3 knockdown and control Hepa 1-6 cells with or without tunicamycin induction was analyzed with flow cytometry. n = 3.
(J) Quantitative real-time PCR analyses of mRNA levels of ATF3 in the livers of *SIRT7*$^{-/-}$ mice and wild-type mice with or without Myc knockdown mediated by AAV8-mediated gene delivery. Mice were analyzed 4 weeks after viral infection. n = 4 mice.

(K-P) Comparison of *SIRT7*$^{-/-}$ mice and wild-type mice with or without ATF3 knockdown mediated by AAV8-mediated gene delivery. Mice were analyzed 4 weeks after viral infection.
(K-M) Quantitative real-time PCR analyses of mRNA levels of indicated genes in the livers. GAPDH was used as an internal control. n = 4-5 mice.
(N) Elisa analyses of plasma levels of IGF-1. n=4-5 mice.
(O and P) Western analyses (O) and quantification (P) for phosphorylated Akt in the livers. n = 3 mice.
Error bars represent standard errors. *$p < 0.05$; **$p < 0.01$; ***$p < 0.001$; ns $p > 0.05$.
See also Figure S4.

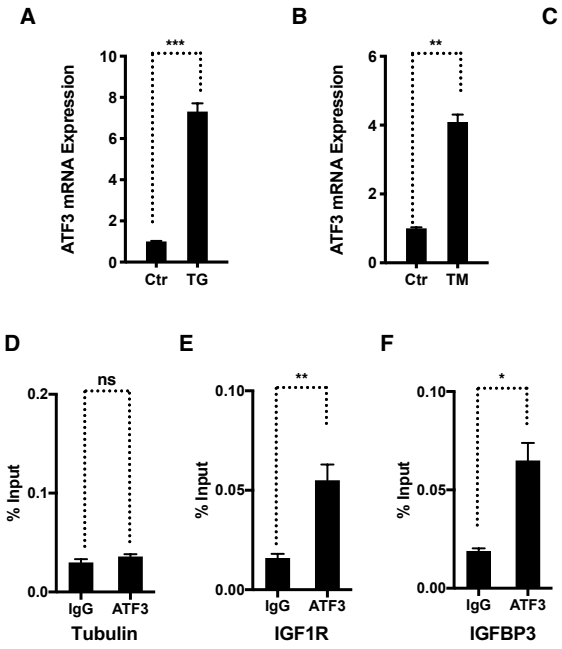

Gene Title	Gene Symbol	Binding Region
IGF1 Receptor	IGF1R	Enhancer
IGF2 mRNA Binding Protein 1	IGF2BP1	Promoter/Enhancer
IGF2 mRNA Binding Protein 3	IGF2BP3	Promoter/Enhancer
IGF2 Receptor	IGF2R	Promoter/Enhancer
IGF Binding Protein 3	IGFBP3	Promoter/Enhancer
IGF Binding Protein 4	IGFBP4	Promoter/Enhancer
IGF Binding Protein 6	IGFBP6	Promoter/Enhancer
IGF Like Family Member 4	IGFL4	Promoter/Enhancer
IGF Like Family Receptor 1	IGFLR1	Enhancer

Figure S4. ATF3 is induced by protein folding stress and binds to the promotors or enhancers of IGF-related genes.

Related to Figure 3.
(A and B) Quantitative real time PCR analyses comparing the mRNA expression of ATF3 in Hepa 1-6 cells treated with or without ER stress inducers thapsigargin (A), tumicamycin (B). n=2-3.
(C) A summary of IGF-related genes as ATF3 targets based on ChIP sequencing analyses using the Harmonizome web portal.
(D-F) ChIP with ATF3 antibody followed by quantitative real-time PCR showing ATF3 occupancy at the promoters of the indicated genes in the mouse liver. n=2-3.
Error bars represent standard errors. * $p < 0.05$; ** $p < 0.01$; *** $p < 0.001$; ns represents $p > 0.05$.

Suppression of the somatotroph axis controls liver damage in NAFLD

The progression from hepatosteatosis to NASH is associated with increased hepatocyte apoptosis and liver damage, which initiate inflammation to clear out dead cells and damaged tissue and to facilitate tissue repair [170,171]. Increased hepatocyte proliferation is one such attempt to repair liver damage and restore loss of mass [172-174], while hepatic stellate cells are also activated and transdifferentiate into myofibroblasts, which produce an excessive amount of extracellular matrix proteins that form fibrous connective tissues to replace normal parenchymal tissues [170]. Hepatic fibrosis, the wound healing process mediated by hepatic stellate cells, is a key feature used to determine the severity of NASH. Suppression of the somatotroph axis in response to ER stress associated with NASH suggests that this branch of the ISR might activate cellular protective program and prevent cell death, resulting in reduced inflammation but compromised parenchymal repair due to repressed hepatocyte proliferation and compensatory fibrosis.

To test this possibility, we examined the physiological effects of suppressing the somatotroph axis on liver damage in NASH. The livers of *SIRT7*$^{-/-}$ mice exhibited increased inflammation (Figure 4A, B), apoptosis (Figure 4A, C), proliferation (Figure 4A, D), and fibrosis (Figure 4A, E), characteristic of the cellular and pathophysiological features of NASH [159,170-173]. The analysis of the single-cell RNA-sequencing data for the livers of wild-type and *SIRT7*$^{-/-}$ mice revealed increased expression of cell cycle genes in hepatocytes of *SIRT7*$^{-/-}$ mice, consistent with increased proliferation of hepatocytes as a way to repair damage and restore loss of mass (Figure S5). ATF3 inactivation in the livers of *SIRT7*$^{-/-}$ mice via AAV8-mediated gene transfer rescued the suppression of the somatotroph axis (Figure 3K-P). Liver terminal deoxynucleotidyl transferase-mediated deoxyuridine triphosphate nick end labeling (TUNEL) staining demonstrated increased frequency of apoptotic cells (Figure 4A, C), while liver Ki67 staining showed increased frequency of proliferating cells (Figure 4A, D) in *SIRT7*$^{-/-}$ mice with ATF3 inactivation compared to *SIRT7*$^{-/-}$ control mice. Compared to *SIRT7*$^{-/-}$ control mice, *SIRT7*$^{-/-}$ mice with ATF3 inactivation showed increased inflammation in the livers, as evidenced by staining of CD68, a marker for macrophages (Figure 4A, B). Hepatic fibrosis as measured with Sirius Red staining was reduced in *SIRT7*$^{-/-}$ mice with ATF3 inactivation (Figure 4A, E). Consistent with these observations, ATF3 KO mice showed increased hepatic apoptosis, liver damage, and inflammation upon liver ischemia/reperfusion injury [175]. These data suggest that suppression of the somatotroph axis prevents hepatocyte apoptosis, liver damage, and inflammation, while suppressing hepatocyte proliferation and parenchymal repair, and promoting compensatory fibrosis (Figure 4F).

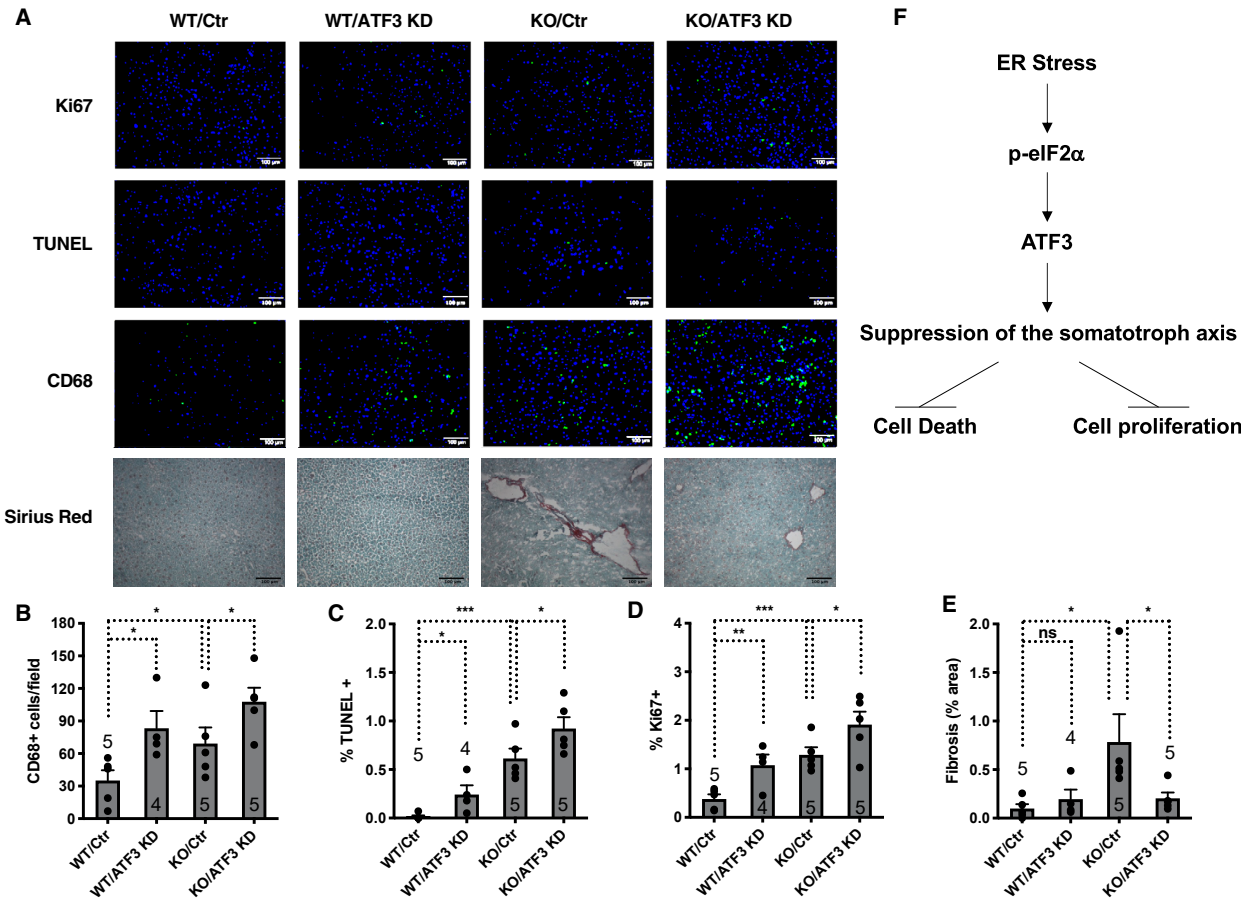

Figure 4. Suppression of the somatotroph axis controls liver damage in NAFLD.

(A-E) Liver sections stained for Ki67, TUNEL, CD68, and Sirius red (A) and their quantifications (B-E) for *SIRT7*$^{-/-}$ mice and wild-type mice with or without ATF3 knockdown mediated by AAV8-mediated gene delivery. Mice were analyzed 4 weeks after viral infection. n = 4-5 mice. Scale bar: 100 μm.

(F) A proposed model. Hepatic ER stress and the ISR induce ATF3 expression and the suppression of the somatotroph axis, leading to reduced hepatocyte death, liver damage, and inflammation, while reducing hepatocyte proliferation and parenchymal repair, resulting in compensatory fibrosis.

Error bars represent standard errors. *p < 0.05; **p < 0.01; ***p < 0.001; ns p > 0.05.

See also Figure S5.

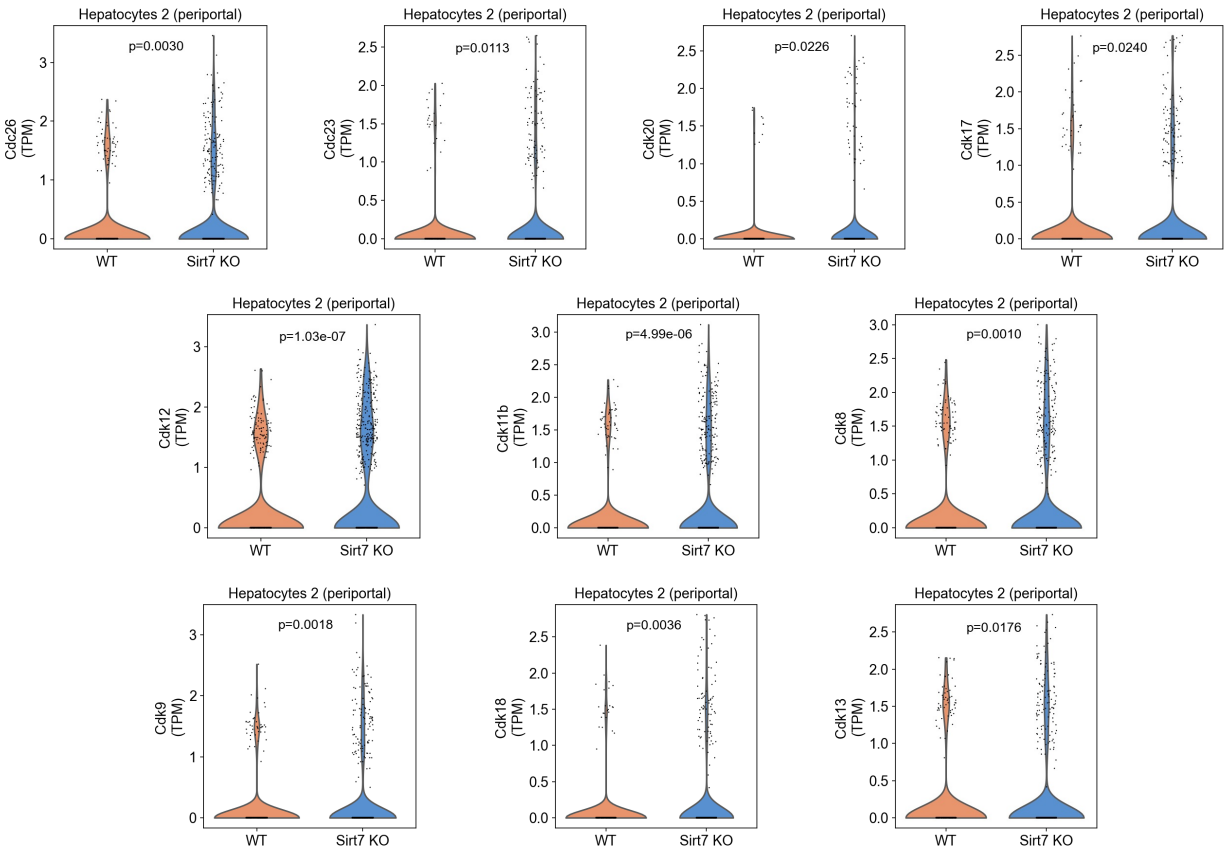

Figure S5. Increased expression of cell cycle genes in hepatocytes of the livers of *SIRT7*$^{-/-}$ mice.

Related to Figure 4.
Violin plots showing the expression of representative cell cycle genes in hepatocytes of the livers of WT and *SIRT7*$^{-/-}$ mice. Each dot represents the gene expression levels in one cell. n=3 mice. P values are false discovery rate-corrected, MAST differential expression test.

Diet-induced NASH mouse models show reduced plasma IGF-1 levels [176-178]. We therefore next tested whether hepatic ER stress and the ISR suppress the somatotroph axis to control liver damage in commonly used preclinical NASH models. Wild-type mice with ATF3 inactivation in the livers via AAV8-mediated gene transfer and the mice treated with control virus were fed a choline-deficient high fat diet (CD-HFD) to induce hepatic steatosis, liver damage, and fibrosis [171] (Figure 5A, B, S6A, B). ATF3 was induced in the livers of mice fed a CD-HFD compared to mice fed a chow diet (Figure 5A, B). Compared to chow fed mice, CD-HFD mice had reduced expression of the somatotroph genes in the livers (Figure S6C, D) and reduced plasma IGF-1 level (Figure 5C). ATF3 inactivation in the livers of CD-HFD fed mice increased the plasma IGF-1 levels (Figure 5C). Staining of liver samples showed increased frequency of Ki67 (Figure 5D, E), TUNEL (Figure 5D, F), CD68 positive cells (Figure 5D, G) and decreased staining of Sirius Red (Figure 5D, H) in CD-HFD mice with ATF3 inactivation compared to CD-HFD control mice. ATF3 inactivation also increased the expression of inflammatory marker genes in the livers of CD-HFD mice (Figure S6E, F).

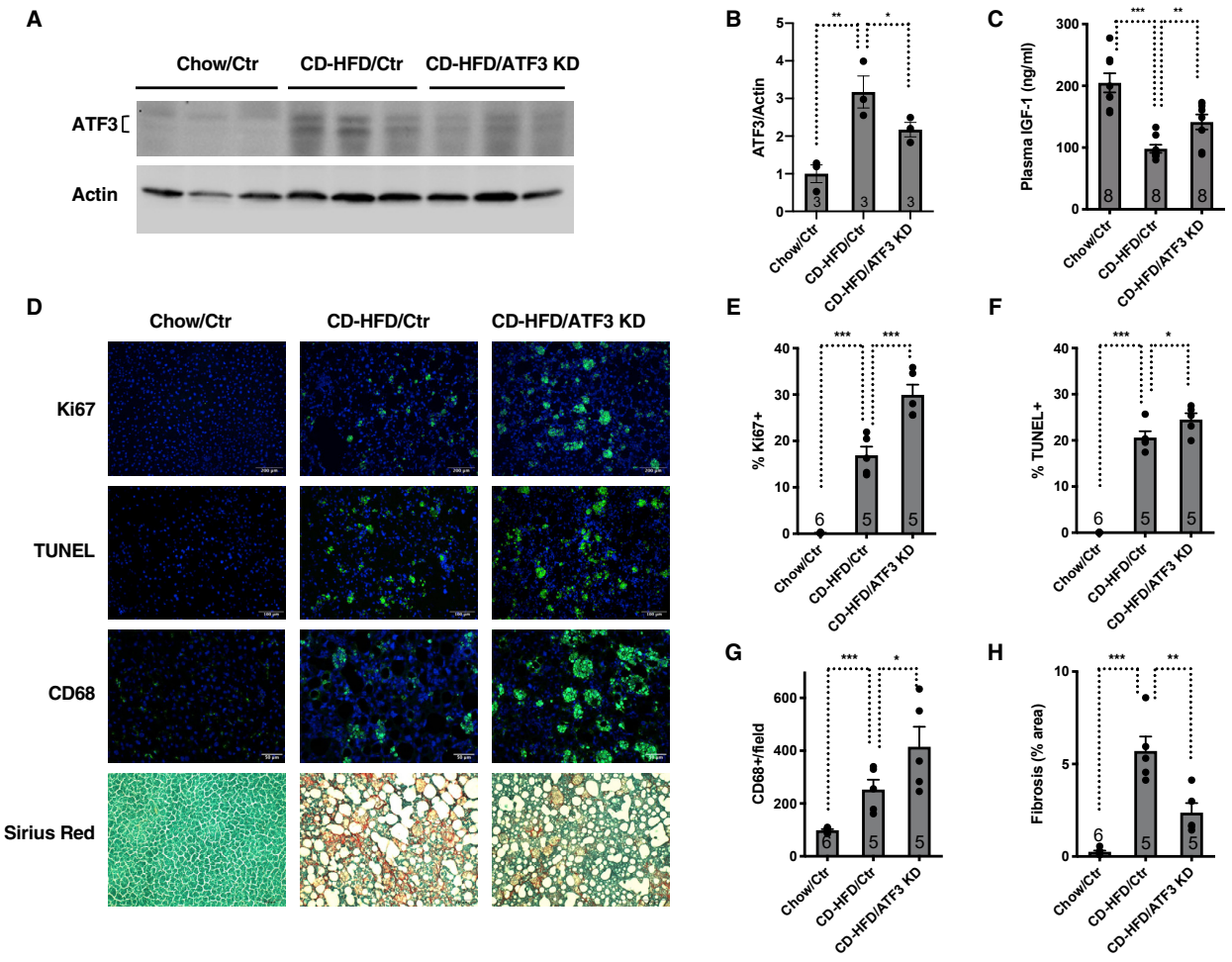

Figure 5. Suppression of the somatotroph axis controls liver damage in mice fed a CD-HFD.

Comparison of wild-type mice with or without ATF3 knockdown in the livers fed a chow diet or a CD-HFD for 8 weeks.
(A and B) Western analyses (A) and quantification (B) of ATF3 in the livers. n = 3 mice.
(C) ELISA analyses of plasma levels of IGF-1. n = 8 mice.
(D-H) Liver sections stained for Ki67, TUNEL, CD68, and Sirius red (D) and their quantifications (E-H). n = 5-6 mice. Scale bars: 200 μm (Ki67), 100 μm (TUNEL, Sirius red), and 50 μm (CD68).
Error bars represent standard errors. *p < 0.05; **p < 0.01; ***p < 0.001.
See also Figure S6.

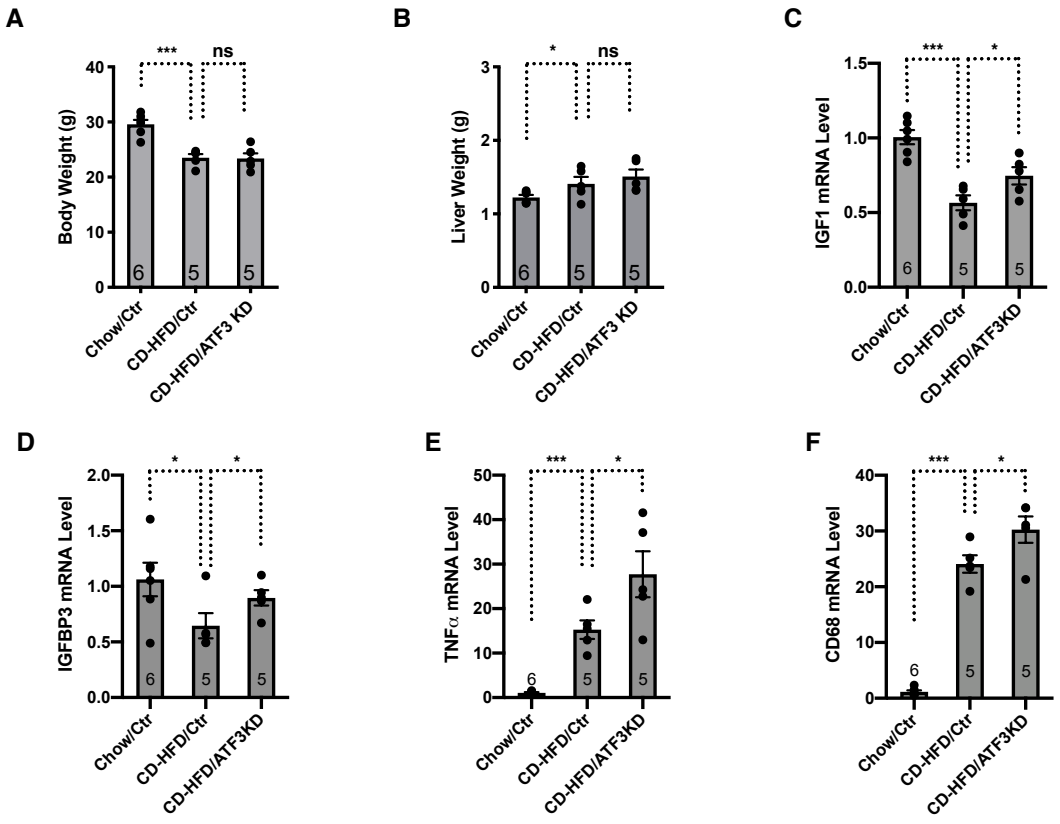

Figure S6. Suppression of the somatotroph axis controls liver damage in mice fed a CD-HFD.

Related to Figure 5.
Comparison of wild type mice with or without ATF3 knockdown in the livers fed a chow diet or a CD-HFD for 8 weeks.
(A) Body weight. n=5-6 mice.
(B) Liver weight. n=5-6 mice.
(C-F) Quantitative real-time PCR analyses of expression of indicated genes in the livers. n=5-6 mice
Error bars represent standard errors. * $p < 0.05$. *** $p < 0.001$. ns represents $p > 0.05$.

To test directly the effects of IGF-1 on liver damage in NASH, we treated either *SIRT7*$^{-/-}$ mice or CD-HFD mice with IGF-1 for 4 weeks. Staining of liver samples showed increased frequency of CD68 positive cells and decreased staining of Sirius Red in *SIRT7*$^{-/-}$ mice (Figure 6A-C) or CD-HFD mice (Figure 6D-F) treated with IGF-1 compared to their respective controls. These results are consistent with the effects of upregulating the somatotroph axis via ATF3 knockdown on liver damage in NASH (Figure 4, 5).

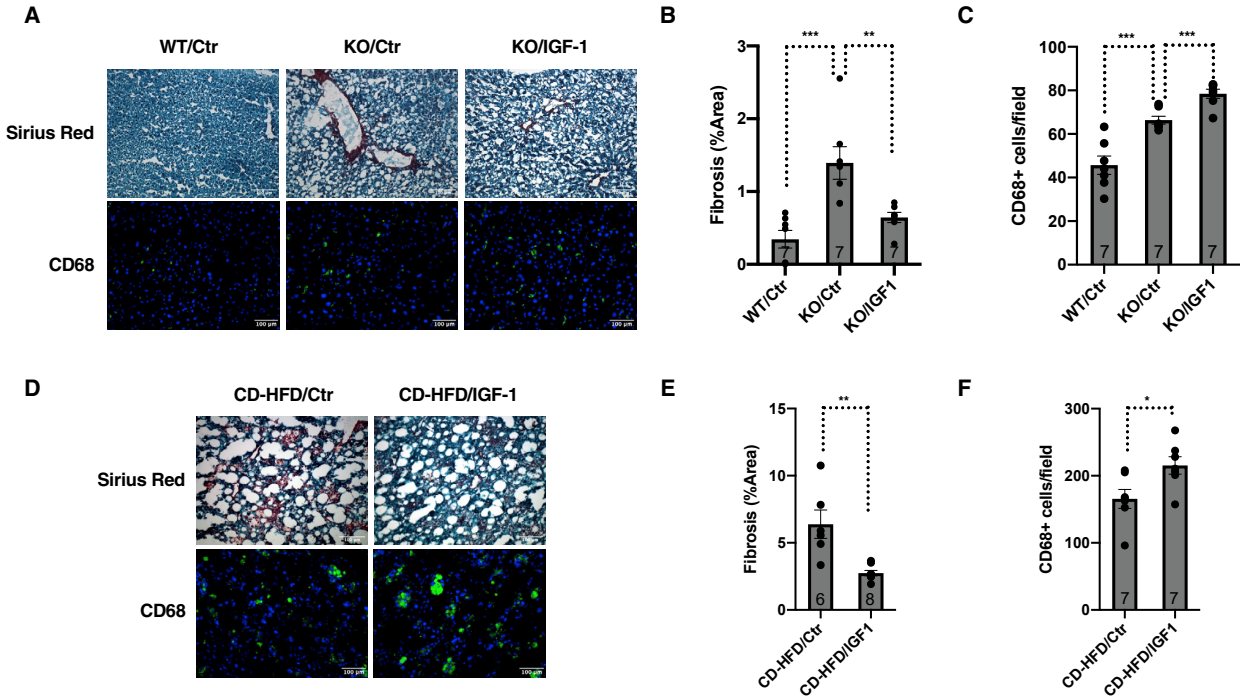

Figure 6. IGF-1 controls liver damage in NAFLD.

(A-C) Comparison of wild-type and *SIRT7*$^{-/-}$ mice treated with or without IGF-1 for 4 weeks. Data shown are liver sections stained for CD68 and Sirius red (A) and their quantifications (B and C). n = 7 mice. Scale bar: 100 μm.
(D-F) Comparison of wild-type mice fed a CD-HFD for 3 weeks followed by treatment with or without IGF-1 for 4 weeks. Data shown are liver sections stained for CD68 and Sirius red (D) and their quantifications (E and F). n = 6-8 mice (E) and 7 mice (F). Scale bar: 100 mm.
Error bars represent standard errors. *p < 0.05; **p < 0.01; ***p < 0.001.

Together, these data are consistent with the model that ATF3 activation represses the somatotroph axis, leading to reduced hepatic apoptosis and inflammation, but decreased hepatic proliferation and increased fibrosis (Figure 4F). Therefore, an effective approach to ameliorate both inflammation and fibrosis, two major indications for effective NAFLD therapeutics, would be targeting an event upstream of the suppression of the somatotroph axis, such as the ER stress.

NAD$^+$ repletion reduces hepatic ER stress and ameliorates liver damage in NAFLD

We took a pharmacological approach to activate SIRT7 and suppress ER stress. NAD$^+$ boosters are emerging to be attractive means to activate sirtuins [179-181]. We treated CD-HFD mice with 78c, an NAD$^+$ booster, for 4 weeks [182] (Figure S7A, B). 78c treatment reduced ER stress and the ISR induction in the liver (Figure 7A, B, C), rescued dysregulated somatotroph gene expression (Figure 7D, E), increased the plasma IGF-1 levels (Figure 7F), reduced hepatic triglyceride content (Figure 7G), reduced hepatic inflammation (Figure 7H-K) and fibrosis (Figure 7J, L).

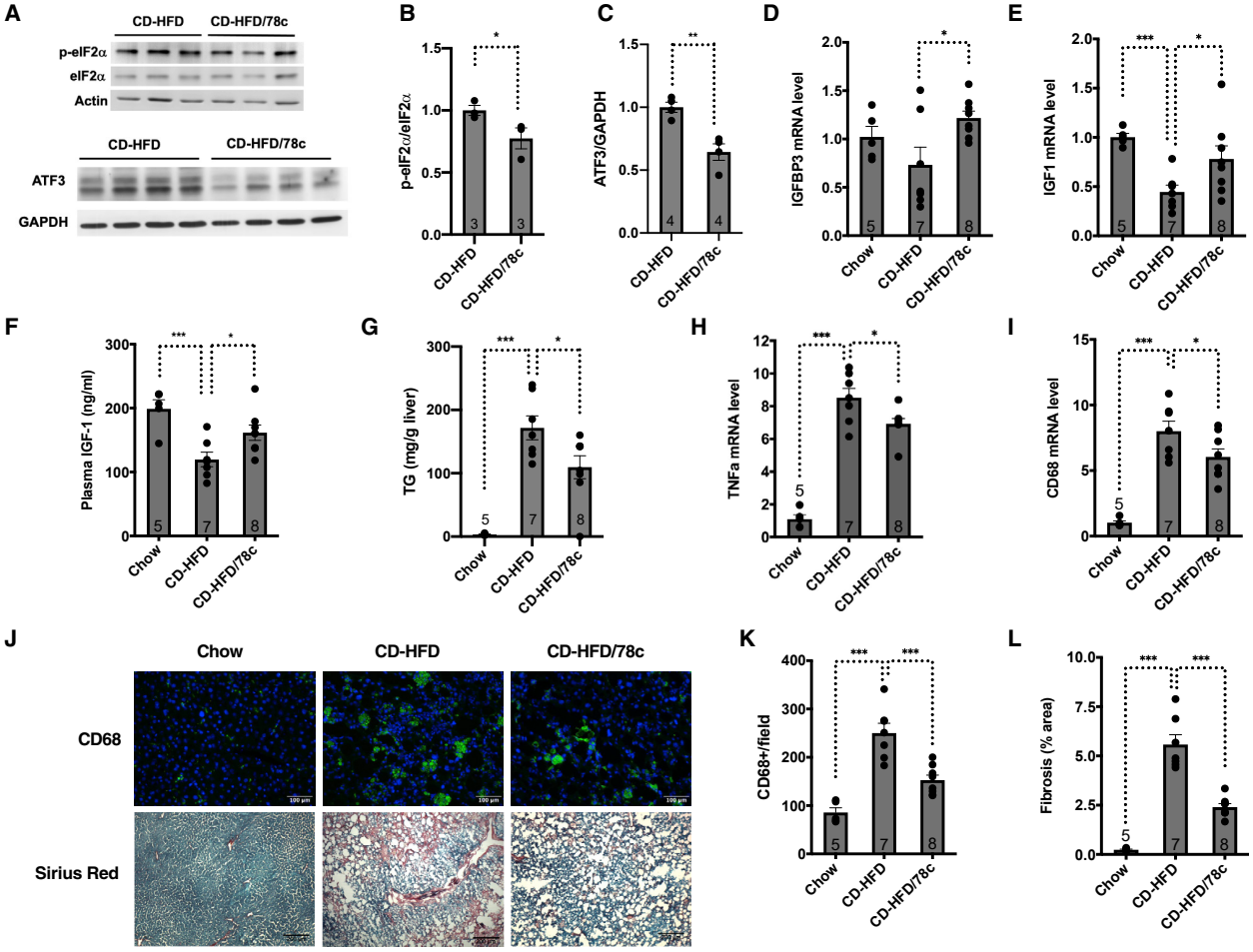

Figure 7. NAD$^+$ repletion ameliorates hepatic ER stress, dysregulated somatotroph axis, and liver damage in NAFLD.

Comparison of mice fed a chow diet or a CD-HFD for 3 weeks followed by treatment with or without 78c for 4 weeks.
(A-C) Western analyses (A) and quantification (B and C) for phosphorylated eIF2a and ATF3 in the livers. n = 3-4 mice.
(D and E) Quantitative real-time PCR analyses for the mRNA levels of indicated genes in the livers. GAPDH was used as an internal control. n = 5-8 mice. (F) ELISA analyses of plasma levels of IGF-1. n = 5-8 mice.
(G) Liver triglyceride quantification. n = 5-8 mice.
(H and I) Quantitative real-time PCR analyses for the mRNA levels of the indicated genes in the livers. GAPDH was used as an internal control. n = 5-8 mice. (J-L) Liver sections stained for CD68 and Sirius red (J) and their quantifications (K and L). n = 5-8 mice. Scale bars: 100 μm (CD68) and 200 μm (Sirius red). Error bars represent standard errors. *$p < 0.05$; **$p < 0.01$; ***$p < 0.001$.
See also Figure S7.

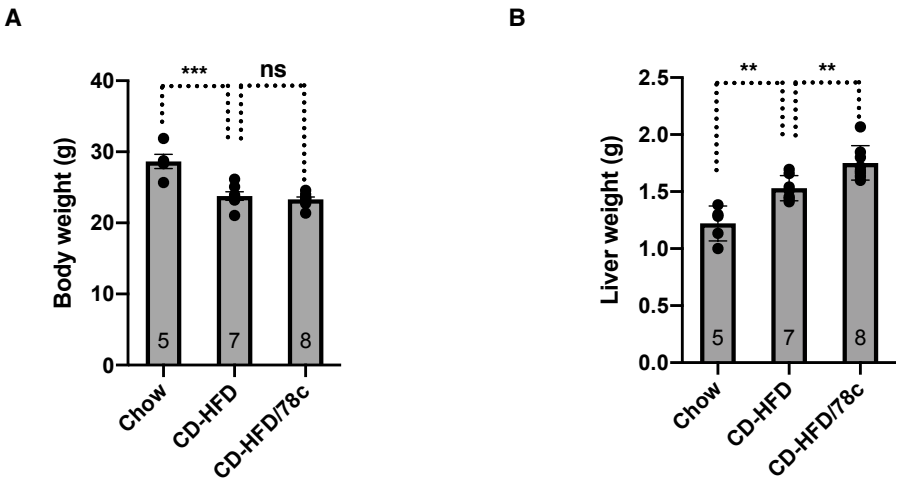

Figure S7. The effects of 78c on CD-HFD mice.

Related to Figure 7.
Mice were fed a chow diet or a CD-HFD for 3 weeks before the treatment with or without 78c for 4 weeks. Data shown are body weight (A) and liver weight (B). n=5-8 mice.

Discussion

Our studies establish suppression of the somatotroph axis as a physiological response to hepatic ER stress that controls liver damage during the progression of NASH. Suppression of the somatotroph axis results in improved hepatocyte survival and reduced inflammation, but repressed hepatocyte proliferation and parenchymal repair, and compensatory fibrosis (Figure 4-6). These findings provide mechanistic insights into the epidemiological observations that suppression of the somatotroph axis is associated with NAFLD patients, in particular the severity of fibrosis [148-157]. These findings also offer an explanation that NAFLD can be ameliorated by calorie restriction at the early stage, which elicits the suppressed somatotroph axis and prevents the hepatocyte cell death and further liver damage [139-147].

Our studies identify a regulatory branch of the hepatic ISR and uncover ATF3 as a stress-induced transcription factor that orchestrates the gene expression of the somatotroph axis. Although ATF3 is known to be induced by ER stress [166], its role in stress response is obscure. We show that ATF3 binds to the promoters or enhances of the somatotroph genes to control their expression (Figure S4C-F, 3A-F). The suppressed somatotroph axis leads to reduced cell proliferation but increased stress resistance to improve cell survival (Figure 3G-I). Thus, this regulatory branch of ISR constitutes a stress response to prevent cell death.

Overnutrition and obesity are strongly associated with NAFLD while calorie restriction is an effective intervention that prevents NAFLD in humans [158,159,183-186]. Sirtuins are nutrient sensors that mediate the responses to calorie restriction and overnutrition [32,33,72-74,187,188]. Indeed, evidence is emerging showing dysregulated sirtuin expression in the livers of NAFLD patients [189] and linking sirtuins to nutritional regulation of PNPLA3, which is strongly linked to NAFLD [190]. SIRT7 alleviates diet-induced NAFLD [73].Therefore, sirtuins are thought to be relevant to the pathogenesis and prevention of NAFLD associated with nutrition and obesity.

Furthermore, dysregulated NAD^+ metabolism has been linked to human NAFLD. For example, the levels of NAMPT, a rate-limiting enzyme for NAD^+ biosynthesis, is reduced in the livers and the plasma of NAFLD patients [191]. NAMPT functions to prevent hepatocyte apoptosis [191]. The NAD^+ level is reduced in the livers of NASH patients [192]. Sirtuins are the major NAD^+ consuming enzymes that mediate the signaling effects of NAD^+ and are thought to be the mediators of NAD^+ metabolism in NAFLD. Indeed, overexpression of SIRT7 rescues diet-induced NAFLD in mice [73].

Given the association of sirtuins to known risk factors of NAFLD, such as diet, obesity, and NAD^+, the prominent NAFLD phenotype in the *SIRT7*$^{-/-}$ mouse model [73,74,164], and the observation that SIRT7 prevents the development of NAFLD by suppressing ER stress [73], a major driver of the progression from NAFLD to NASH [160], the *SIRT7*$^{-/-}$ mouse model is relevant to human NASH, although human GWAS data linking SIRT7 to NAFLD have not emerged yet. Indeed, our single-cell RNA-sequencing analysis provided further support that the *SIRT7*$^{-/-}$ mouse model develops NAFLD (Figure 1B, C, S1D, E). Using

the *SIRT7*$^{-/-}$ mouse model, we showed that suppression of the somatotroph axis reduces hepatic inflammation but promotes fibrosis (Figure 4, 6A-C). This finding was further validated using the CD-HFD mouse model (Figure 5, 6D-F, 7, S6, S7). The consistent findings in both mouse models of NAFLD further support the relevance of the *SIRT7*$^{-/-}$ mouse model to NAFLD.

NAD^+ boosting has demonstrated the therapeutic potential for a number of diseases [179-181]. Our studies show that NAD^+ boosting via 78c can ameliorate NASH, a prevalent metabolic disease that needs a cure, at least in part by modulating the hepatic ISR and the somatotroph axis in mouse models (Figure 7), demonstrating the therapeutic potential of modulating this pathway. Suppression of the somatotroph axis in response to ER stress uncouples inflammation and fibrosis (Figure 4-6), providing a basis for combination therapies or targeting an initiating event, such as ER stress, for this metabolic disease (Figure 7).

Materials and Methods

Mice

SIRT7$^{-/-}$ mice have been described previously [72,73]. For a diet-induced NAFLD mouse model, C57BL/6 male mice were fed with choline-deficient high-fat diet (Research Diet, A06071302) consisting of 60 kcal% fat with 0.1% methionine and no added choline for 3 weeks before either 78c treatment or IGF-1 treatment. 78c was administered to mice by intraperitoneal injection (10 mg/kg/dose) twice daily for 4 weeks. Control mice received vehicle (5% DMSO, 15% PEG400, 80% of 15% hydroxypropyl-g-cyclodextrin (in citrate buffer pH 6.0)) injections. IGF-1 (Pepro Tech) dissolved in 0.1% BSA/PBS was administered to mice by subcutaneous injection (20 µg/kg/day) for 4 weeks. All mice were housed on a 12:12 hr light:dark cycle at 25°C and were given free access to food and water. All animal procedures were in accordance with the animal care committee at the University of California, Berkeley.

Cell culture

Hepa 1-6 cells were acquired from cell culture facility at the University of California, Berkeley. Cells were cultured in advanced Dulbecco's modified Eagle's medium (Gibco) supplemented with 10% FBS (Gibco). For ER stress induction, cells were treated with tunicamycin (Sigma, 2µg/ml) or thapsigargin (Sigma, 0.1µM) for 24 hr before biochemical analysis. For ATF3 knockdown, Hepa 1-6 cells were transfected with AllStars Negative Control siRNA (Qiagen, 1027281) or ATF3 siRNA (Qiagen, GS11910) using RNAiMAX (Invitrogen, 13778100) according to manufacture's instruction. To generate Hepa 1-6 cells with stable ATF3 knockdown, cells were infected with lentivirus. For lentiviral packaging, 293T cells were co-transfected with packaging vectors (pCMV-dR8.2 dvpr and pCMV-VSV-G) and the pLKO.1-ATF3 shRNA (Sigma, TRCN0000082129, TRCN0000082132) or control construct. Viral supernatant was harvested after 48 hours and 72 hours after transfection, as described previously [193]. For transduction, cells were incubated with virus-containing supernatant in the presence of 10 µg/mL polybrene. After 48 hours, infected cells were selected with puromycin (4µg/mL). For cell proliferation, $0.3x10^6$ cells were seeded in a 6-well plate. Two days later, 20% cells were passaged to a new well and were counted 24 hours later.

Primary hepatocytes were suspended in plating medium (DMEM low glucose, 5% FBS and 1%Pen/Strep) and plated on collagen-coated cell culture plates (Sigma-Aldrich C3867-1VL). After 3 hours, it was changed to maintenance media (Williams E media, 1% Glutamine and 1% Pen/Strep). The next day cells were treated with tunicamycin for 24 hours (Sigma, 4µg/ml) before analysis.

Apoptosis assay

Apoptotic cells were assayed using propidium iodide (BioLegend) and FITC Annexin V staining (BioLegend) according to the manufacturer's instruction (BioLegend). All data were collected on an LSR Fortessa (BD Bioscience), and data analysis was performed with FlowJo (TreeStar).

Chromatin immunoprecipitation
Cells were prepared for ChIP as previously described [194], with the exception that DNA was washed and eluted using a QIAprep Spin Miniprep kit (Qiagen) rather than by phenol-chloroform extraction. For ChIP with mouse livers, 150 mg mouse liver were minced and dounce homogenized with 10 strokes in hypotonic lysis buffer (10mM HEPES, pH7.5, 10mM KCl, 1.5mM MgCl2, 250mM Sucrose, 0.5% NP40, and protease inhibitor cocktail). Lysates were filtered through a 100um cell strainer and spin at 1500g for 5 min. Lipid and cytoplasmic fractions were removed and the nuclear pellet was resuspended in lysis buffer, cross-linked with fresh formaldehyde (1%) for 5 min at room temperature, quenched with glycine (125mM), and washed twice with PBS.

Affymetrix microarray
Total RNA was isolated from the livers of wild type and *SIRT7*$^{-/-}$ mice using an RNA isolation kit (Qiagen). Microarray hybridizations were performed at the University of California, Berkeley Functional Genomics Laboratory using Affymetrix GeneChip mouse 430As according to the instructions of the manufacturer (Affymetrix). RMA normalization was applied and the limma package was used to identify the differentially expressed genes. Differentially expressed genes were selected using the Benjamini-Hochberg method to control the FDR at 15%.

Single-cell RNA-sequencing of livers using 10x Genomics Chromium.
Hepatocytes and non-parenchymal cells (NPCs) were isolated by a two-step collagenase perfusion method [195]. Briefly, after the inferior vena cava was cannulated with a 25 gauge catheter and the portal vein was cut, the liver was perfused at 10 ml/minute with Liver Perfusion Medium (Gibco 17701-038) at 37°C for 5 minutes, followed by perfusion with collagenase type IV (Worthington LS004188) in HBSS (GIBCO) at 37°C for 5 minutes. The liver was dissected out and transferred to petri dish with William E medium (Gibco 12551-032) containing 200 mM L-glutamine, 1% pen/strep and 1% non-essential amino acid. Then gently shake out the cells from liver capsule. The released liver cells were passed through a 100 µm filter. Hepatocytes were separated from NPCs by low-speed centrifugation (50 x g, 4 minutes, 3x, brake=2) and further purified by Percoll gradient centrifugation (50% v/v) to remove dead cells [196]. NPCs were pelleted from supernatant by centrifugation (300 xg, 10 minutes) then purified by Percoll gradient centrifugation (33% v/v) to remove dead cells [197]. Cell viability was confirmed by trypan blue exclusion. 3000 hepatocytes and 3000 NPCs were mixed and used directly for scRNA-seq analysis using 10X Genomics Chromium Single-Cell 3' according to the manufacturer's instructions.

10x Genomics single-cell RNA-sequencing data pre-processing, UMAP analysis, and identification of cell clusters.
RNA reads from sequencing were demultiplexed and aligned to mouse transcriptome (mm10) using the Cell Ranger software (10x Genomics, v.6.0.0). The Scanpy Python package (v.1.6.0) was used for the pre-processing of the single-cell RNA seq data [198]. Cells with less than 500 unique genes or more than 5% mitochondrial genes were removed. Genes detected in less than 3 cells were excluded. We included 11610 cells with 3270 cells from wild type and 8340 cells from *SIRT7*$^{-/-}$, and 16623 genes for further analysis. The data was normalized such that every cell has 10,000 counts and then log

transformed with an offset of 1. The batch correction was done by the bbknn batch-alignment algorithm . We computed the highly variable genes with the top 1,000 genes and the flavor set to 'cell_ranger'. The highly variable genes were used for principal components analysis. The data was visualized by UMAP (Uniform Manifold Approximation and Projection) projection using Scanpy [198]. Unsupervised clustering was done by the Leiden algorithm [199] with a resolution of 0.35. Marker genes for each cluster were calculated by Wilcoxon rank-sum test. The cell identity of each cluster was determined by comparing the marker genes of each cluster with the marker genes identified in the literature.

Differential gene expression analysis, bar plots, violin plots, and dot plots for gene expression in single cells, and pathway enrichment analysis.

Adaptive thresholding of the single-cell gene expression data was performed with the MAST R package (v1.12.0), and differential gene expression analysis of wild type and *SIRT7*$^{-/-}$ cells from each cluster using a hurdle model with the wild type cells as the reference [200]. To visualize the expression of genes, log-normalized expressions of genes were extracted from the data after adaptive thresholding and plotted for every cell with a violin plot and an overlying strip plot by the Seaborn Python package (v.0.9.0). The bar plots were generated by Seaborn. The UMAP plots, dot plots, and track plots were generated by Scanpy. The GSEAPY Python package (v.0.10.3) was used for pathway enrichment analysis.

Quantitative Real-Time PCR

RNA was isolated from cells or tissues using Trizol reagent (Invitrogen) following the manufacturer's instructions. cDNA was generated using the qScript cDNA SuperMix (Quanta Biosciences). Gene expression was determined by quantitative real time PCR using Eva qPCR SuperMix kit (BioChain Institute) on an ABI StepOnePlus system. All data were normalized to GAPDH expression.

AAV8-mediated gene transfer

For AAV8-mediated gene transfer to the mouse liver, Myc knockdown target sequence was cloned into dsAAV-RSVeGFP-U6 vector. AAV8 for knocking down Myc was produced by Vigene biosciences. AAV8 for knocking down ATF3 was acquired from Vector biolabs. Myc knockdown target sequence: 5'-CCCAAGGTAGTGATCCTCAAA-3'. ATF3 knockdown target sequence: 5'-TGCTGCCAAGTGTCGAAACAA-3'. Each mouse was injected with 3×10^{11} genome copies of virus via tail vein. Mice were characterized four weeks after viral infection (wild-type and *SIRT7*$^{-/-}$ mice) or eight weeks after viral infection (CD-HFD mice).

Plasma IGF-1 levels

To detect IGF-1 in the plasma, the plasma was pretreated with acid-ethanol extraction solution to release IGF-1 from binding proteins. Briefly, 120 μL of acid-ethanol extraction buffer (hydrochloric acid:water:ethanol = 1:4:35, v/v/v) was added to 30 μL of plasma. The extract was incubated for 30 min at room temperature with shaking. The extract was centrifuged at 10,000 rpm for 5 min and 100 μL of supernatant was collected. 200 uL of Tris buffer (pH = 7.6) was added to the supernatant. IGF-1 was detected using IGF-1

Mouse ELISA Kit (Invitrogen).

Immunohistochemistry
Tissue sections (5 μm) were mounted on glass slides. Slides were fixed with 10% formalin. Tissue processing and immunohistochemistry was performed on sections. Primary antibodies were: mouse anti-CD68 (Biolegend, 137001); Ki67 (Biolegend, 652409). After overnight incubation, primary antibody staining was revealed using fluorescence conjugated secondary antibodies. Nuclei were counter stained using DAPI. Images were taken with Zeiss AxioImager microscope. The positive cells were manually counted or counted using ImageJ.

Fibrosis staining
Liver sections were fixed with 10% formalin and then stained with Sirius Red (Sigma)/Fast Green (Sigma). Images were taken with Zeiss AxioImager microscope. The positive area was quantified using ImageJ.

TUNEL staining
Apoptosis was detected with Apo-Brdu *in situ* DNA fragmentation assay kit according to the manufacturer's instruction (Biovision). Nuclei were counter stained using DAPI. TUNEL-positive cells were imaged using Zeiss AxioImager microscope.

Western Blot
Tissues or cells were homogenized in a lysis buffer that contained protease inhibitor, and total protein was extracted with gentle rotation for 30 min at 4˚C. The extract was centrifuged at 15,000 g for 15 min at 4°C. Supernatants were collected and total protein was quantified with BCA assay (Thermo Scientific, 23225). Proteins were resolved by SDS-PAGE and transferred to nitrocellulose membranes (Bio-Rad), which was incubated with specific primary antibodies and horseradish peroxidase-conjugated secondary antibodies, and enhanced chemiluminescence substrate (PerkinElmer, NEL103001EA), and visualized using ImageQuant™ LAS 4000 (GE Healthcare).

Triglyceride Quantification
Triglycerides were extracted from liver tissues as described [201]. Extracted triglyceride was quantified in accordance with the manufacturer's instruction (Wako Diagnostics).

QUANTIFICATION AND STATISTICAL ANALYSIS
Statistical analysis was performed with Student's *t* test (Excel) unless specified. Wilcoxon rank-sum test for single-cell RNA sequencing analysis was performed using the SciPy Python package (v.1.4.1). Data are presented as means and error bars represent standard errors. In all corresponding figures, * represents $p < 0.05$. ** represents $p < 0.01$. *** represents $p < 0.001$. ns represents $p > 0.05$. Replicate information is indicated in the figures.

REAGENT or RESOURCE	SOURCE	IDENTIFIER
Antibodies		
p-eIF2α (Ser52) polyclonal antibody	Invitrogen	Cat# 44728G, RRID:AB_1500038
eIF2α antibody	CST	Cat# 9722, RRID: AB_2230924
Phospho-Akt (Ser473) antibody	CST	Cat# 9271, RRID:AB_329825
Akt antibody	CST	Cat# 9272, RRID:AB_329827
Actin antibody	Sigma	Cat# A2066, RRID:AB _476693
GAPDH antibody	CST	Cat# 5174, RRID: AB_10622025
Mouse Growth Hormone R/GHR Antibody	R&D	Cat# AF1360, RRID:AB_2111403
Mouse FGF acidic/FGF1 Antibody	R&D	Cat# AF4686, RRID: AB_2924726
ATF-3 (D2Y5W) Rabbit antibody	CST	Cat# 33593S RRID: AB_2799039
Normal Rabbit IgG	CST	Cat# 2729S, RRID: AB_1031062
Purified anti-mouse CD68 Antibody	BioLegend	Cat#137001, RRID: AB_2044003
Goat anti-Rat IgG (H+L) cross-absorbed secondary antibody, DyLight 488	ThermoFisher Scientific	Cat# SA5-10018. RRID: AB_2556598
FITC anti-mouse Ki-67 Antibody	BioLegend	Cat# 652409, RRID: AB_2562140
Chemicals, Peptides, and Recombinant Proteins		
78c (CD38 inhibitor)	MedChemExpress	Cat#: HY-123999 CAS#:1700637-55-3
Dimethyl Sulfoxide (DMSO)	Sigma	Cat# D8418
Polyethylene glycol 400 (PEG400)	Sigma	Cat# PX1286B
Hydroxypropyl-g-cyclodextrin	Santa Cruz biotechnology	Cat# sc-238090A
Recombinant human IGF1	PeproTech	Cat# 100-11
Bovine Serum Albumin	Sigma	Cat# A7906
Dulbecco's Modification of Eagle's Medium	Gibco	Cat# 11995065
Dulbecco's Modification of Eagle's Medium (low glucose)	Gibco	Cat# 11885-084
Williams E media	Gibco	Cat# 12551-032
Liver Perfusion Medium	Gibco	Cat# 17701-038

Collagenase type IV	Worthington	Cat# LS004188
L-Glutamine	Gibco	Cat# 25030081
Non-essential amino acid (100X)	Gibco	Cat# 11140-050
Percoll™ PLSU	Cytiva	Cat# 17544702
Fetal Bovine Serum	Invitrogen	Cat#10437-028
Tunicamycin	Sigma	Cat# T7765
Thapsigargin	Sigma	Cat# T9033
RNAiMAX	Invitrogen	Cat# 13778100
Sirius Red (Direct Red 80)	Sigma	Cat# 365548
Fast green	Fisher Chemical	Cat# F99-10
qScript™ cDNA SuperMix	Quanta Biosciences	Cat# 95048
qPCR SuperMix kit	BioChain Institute	Cat# K5052400
Penicillin Streptomycin Solution (100x)	Invitrogen	Cat# 15140122
Collagen, type I solution from rat tail	Sigma	Cat# C3867-1VL
Trypsin-EDTA (0.25%)	Gibco	Cat# 25200056
TRIzol Reagent	Invitrogen	Cat# 15596026
Lipofectamine 2000	Invitrogen	Cat# 11668019
HEPES	Gibco	Cat# 15630080
HBSS, calcium, magnesium, no phenol red	Gibco	Cat# 14025092
HBSS, no calcium, no magnesium, no phenol red	Gibco	Cat# 14175095
Western (blotting) Lightning Plus-ECL substrate	Perkin Elmer	Cat# NEL103E001EA
DAPI (4',6-diamidino-2-phenylindole, dihydrochloride)	Thermo Fisher Scientific	Cat#62247
Propidium Iodide Solution	Biolegend	Cat#421301
FITC Annexin V	BioLegend	Cat# 640906
Formaldehyde	Thermo Fisher Scientific	Cat# F79-500
Critical Commercial Assays		
QIAprep Spin Miniprep kit	Qiagen	Cat# 27106X4
10x Genomics Single Cell 3' reagent kits v3	10x Genomics	Cat# PN-1000075
IGF-1 Mouse ELISA Kit	Invitrogen	Cat# EMIGF1
Apo-Brdu in situ DNA fragmentation assay kit	Biovision	Cat# K401
Pierce™ BCA Protein Assay Kit	Thermo Scientific	Cat# 23225
L-Type Triglyceride M Enzyme Color A	FUJIFILM Wako Diagnostics	Cat# 996-02895
L-Type Triglyceride M Enzyme Color B	FUJIFILM Wako Diagnostics	Cat# 992-02995
Deposited Data		
SIRT7liver		GEO: GSE216996

Experimental Models: Cell Lines		
Hepa 1-6	UC Berkeley Cell Culture Facility	
HEK293T	ATCC	CRL-3216
Experimental Models: Organisms/Strains		
Mouse: SIRT7 KO	[73]	
Mouse: C57BL/6J	National Institute on Aging	
Oligonucleotides		
Primer GAPDH Forward: ACCCAGAAGACTGTGGATGG Reverse: ACACATTGGGGGTAGGAACA	IDT (integrated DNA technologies)	N/A
Primer GHR Forward: ATTCACCAAGTGTCGTTCC Reverse: TCCATTCCTGGGTCCATTCA	IDT (integrated DNA technologies)	N/A
Primer FGF1 Forward: GGCCAGAAAGCCATCTCGTT T Reverse: TAGCGCAGCCAATGGTCAA	IDT (integrated DNA technologies)	N/A
Primer EGFR Forward: GGAAACCGAAATTTGTGCTAC G Reverse: GCCTTGCAGTCTTTCTCAGCT C	IDT (integrated DNA technologies)	N/A
Primer FGFR4 Forward: GGCTATGCTGTGGCCGCACT Reverse: GGTCTGAGGGCACCACGCTC	IDT (integrated DNA technologies)	N/A
Primer IGFBP1 Forward: TCGCCGACCTCAAGAAATGG Reverse: GGATGTCTCACACTGTTTGCT	IDT (integrated DNA technologies)	N/A
Primer IGF-1 Forward: TGCTTGCTCACCTTCACCA Reverse: CAACACTCATCCACAATGCC	IDT (integrated DNA technologies)	N/A

Primer IGFBP3 Forward: AACATCAGTGAGTCCGAGG Reverse: AACTTTGTAGCGCTGGCTG	IDT (integrated DNA technologies)	N/A
Primer IGF-1R Forward: ACGACAACACAACCTGCGT Reverse: AACGAAGCCATCCGAGTCA	IDT (integrated DNA technologies)	N/A
Primer ATF3 Forward: AGCCTGGAGCAAAATGATGC TT Reverse: AGGTTAGCAAAATCCTCAAAC AC	IDT (integrated DNA technologies)	N/A
Primer TNFa Forward: CTATGGCCCAGACCCTCACA CTC Reverse: GCTGGCACCACTAGTTGGTT GTCTT	IDT (integrated DNA technologies)	N/A
Primer CD68 Forward: AGGTTGTGACGGTACCCATC Reverse: TTGCATTTCCACAGCAGAAG	IDT (integrated DNA technologies)	N/A
Primer IGFBP3 ChIP Forward: GTTCTCGCTGGGAAATGCCT Reverse: TCAGCGCCTGTGTACTTTGT	IDT (integrated DNA technologies)	N/A
Primer IGF-1R ChIP Forward: GGGAATTTCGTCCCAAATAAA AGGA Reverse: GAGAGAAACACGAGCCCCC	IDT (integrated DNA technologies)	N/A
Primer Tubulin ChIP Forward: AGACGGAAGAGAACACTGCG Reverse: CTTCATCGGGCTTCAGTCGT	IDT (integrated DNA technologies)	N/A
ATF3 siRNA TGCTGCCAAGTGTCGAAACA A	Qiagen	Cat# GS11910
Control siRNA	Qiagen	Cat# 1027281

Myc siRNA CCCAAGGTAGTGATCCTCAAA	[73]	
Recombinant DNA		
pCMV-dR8.2 dvpr	Addgene	Plasmid: #8455
pCMV-VSV-G	Addgene	Plasmid: #8454
pLKO.1-ATF3	Sigma	TRCN0000082129 TRCN0000082132
dsAAV-RSVeGFP-U6	[73]	
dsAAV-RSVShMyc	[73]	
Ad-m-ATF3-shRNA	Vector Biolabs	Cat# shADV-253206
Software and algorithms		
Cell Ranger (v.6.0.0)	10X Genomics	
Scanpy Python package (v.1.6.0)	[198]	https://github.com/scverse/scanpy
Bbknn batch-alignment algorithm		https://github.com/Teichlab/bbknn
Leiden algorithm	[199]	https://github.com/vtraag/leidenalg
MAST R package (v.1.12.0)	[200]	https://github.com/RGLab/MAST
Seaborn Python package (v.0.9.0)		https://seaborn.pydata.org/citing.html
GSEAPY Python package (v.0.10.3)		https://github.com/zqfang/GSEApy/releases
ImageJ	[202]	https://imagej.nih.gov/ij/
iVision (v.4.5.6 r4)	BioVision Technologies	https://www.biovis.com
GraphPad Prism	GraphPad	https://www.graphpad.com/
Other		
Choline-deficient high fat diet	Research Diet	Cat# A06071302

Chapter 3: Concluding Remarks and Future Directions

This dissertation aimed to advance our understanding of the biology of fatty liver disease and to develop a new therapeutic approach. Nonalcoholic fatty liver disease (NAFLD) is a metabolic disorder that is closely associated with obesity and abnormal nutrient sensing. Through the use of cutting-edge technologies, including next-generation sequencing, we elucidated the interaction between ER stress and the somatotroph axis in liver damage during the progression of NAFLD in both genetic and diet-induced fatty liver mouse models. Our findings provide important new insights into the pathogenesis of NAFLD and may lead to the development of novel therapeutic strategies.

In Chapter 1, we critically reviewed and summarized the current understanding of nutrient sensing and oxidative stress. We explored the implications of preventing tissue dysfunction and stem cell deterioration in the context of aging and metabolic diseases, emphasizing the importance of nutrient sensors in disease manifestation. By highlighting the key role of nutrient sensing in disease pathology, this chapter sets the foundation for the next chapter, which will delve into a new mechanism by which the nutrient-sensing pathway and the integrated stress response contribute to liver damage during the progression of NAFLD.

In Chapter 2, we reported a novel regulatory pathway that controls liver inflammation and fibrosis during the progression of NAFLD. Our study focused on the nutrient sensor SIRT7, which inhibits ER stress and prevents the progression of fatty liver disease. We began by conducting single-cell RNA-seq analysis on livers from SIRT7 KO mice, which revealed reduced Igf1 expression in hepatocytes. Further examination of SIRT7 KO livers showed that the somatotroph axis and downstream signaling were suppressed, which we also observed in a diet-induced NAFLD mouse model. Mechanistically, we found that elevated ER stress in NAFLD activates ATF3, a stress-induced transcription factor, which binds to the regulatory regions of IGF-related genes and suppresses somatotroph gene expression in hepatocytes. This suppression of the somatotroph axis prevents NAFLD-associated cell proliferation and cell death in the liver. To further investigate this mechanism, we infused human recombinant IGF-1 and found that it directly impacted liver damage by reducing liver fibrosis but enhancing inflammation. Most importantly, we found that pharmacological activation of SIRT7 via NAD^+ boosting using 78c reversed the suppressed somatotroph axis and ameliorated liver damage in the diet-induced NAFLD mouse model. These findings provide crucial insights into a potential therapeutic strategy for treating NAFLD.

This work has revealed the therapeutic potential of activating SIRT7 through NAD^+ boosting in the prevention of liver damage in the context of NAFLD. NMN supplementation, which boosts NAD^+ levels, has been shown to improve muscle insulin sensitivity in prediabetic women [124]. We are excited to take the next steps and explore the possibility of using NAD^+ boosting to ameliorate liver damage in NAFLD patients. Currently, there is no effective pharmacological treatment for NAFLD, with lifestyle changes being the only recommended approach. NAD^+ supplementation has the potential

to be the first pharmacological intervention capable of effectively preventing disease progression. This highlights the importance of our work, which provides crucial insights into the potential for NAD^+ boosting as a novel therapeutic strategy for NAFLD.

References

1. Mu W-C, Chen D. Chapter 22 - Nutrient sensing, the oxidative stress response, and stem cell aging. In: Sies H, ed. *Oxidative Stress*. Academic Press; 2020:427-446.
2. Ohkubo R, Mu WC, Wang CL, et al. The hepatic integrated stress response suppresses the somatotroph axis to control liver damage in nonalcoholic fatty liver disease. *Cell reports*. Dec 13 2022;41(11):111803. doi:10.1016/j.celrep.2022.111803
3. McCay CM, Crowell MF, Maynard LA. The effect of retarded growth upon the length of life span and upon the ultimate body size. *Journal of Nutrition*. Jul 1935;10:63-79.
4. Colman RJ, Anderson RM, Johnson SC, et al. Caloric restriction delays disease onset and mortality in rhesus monkeys. *Science (New York, NY)*. 2009;325(5937):201-204. doi:10.1126/science.1173635
5. Jiang JC, Jaruga E, Repnevskaya MV, Jazwinski SM. An intervention resembling caloric restriction prolongs life span and retards aging in yeast. *FASEB journal : official publication of the Federation of American Societies for Experimental Biology*. Nov 2000;14(14):2135-7. doi:10.1096/fj.00-0242fje
6. Klass MR. Aging in the nematode Caenorhabditis elegans: major biological and environmental factors influencing life span. *Mechanisms of ageing and development*. Nov-Dec 1977;6(6):413-29.
7. Masoro EJ. Overview of caloric restriction and ageing. *Mechanisms of ageing and development*. Sep 2005;126(9):913-22. doi:10.1016/j.mad.2005.03.012
8. Blackwell BN, Bucci TJ, Hart RW, Turturro A. Longevity, body weight, and neoplasia in ad libitum-fed and diet-restricted C57BL6 mice fed NIH-31 open formula diet. *Toxicologic pathology*. Sep-Oct 1995;23(5):570-82.
9. Weindruch RH, Kristie JA, Cheney KE, Walford RL. Influence of controlled dietary restriction on immunologic function and aging. *Federation proceedings*. May 1979;38(6):2007-16.
10. Ingram DK, Weindruch R, Spangler EL, Freeman JR, Walford RL. Dietary restriction benefits learning and motor performance of aged mice. *Journal of gerontology*. Jan 1987;42(1):78-81.
11. Lee BC, Kaya A, Gladyshev VN. Methionine restriction and life-span control. *Annals of the New York Academy of Sciences*. Jan 2016;1363:116-24. doi:10.1111/nyas.12973
12. Mirzaei H, Raynes R, Longo VD. The conserved role of protein restriction in aging and disease. *Current opinion in clinical nutrition and metabolic care*. Jan 2016;19(1):74-9. doi:10.1097/MCO.0000000000000239
13. Schulz TJ, Zarse K, Voigt A, Urban N, Birringer M, Ristow M. Glucose restriction extends Caenorhabditis elegans life span by inducing mitochondrial respiration and increasing oxidative stress. *Cell metabolism*. Oct 2007;6(4):280-93. doi:10.1016/j.cmet.2007.08.011
14. Beckman KB, Ames BN. The free radical theory of aging matures. *Physiological reviews*. Apr 1998;78(2):547-81. doi:10.1152/physrev.1998.78.2.547

15. Harman D. Aging: a theory based on free radical and radiation chemistry. *Journal of gerontology*. Jul 1956;11(3):298-300.
16. Pomatto LCD, Davies KJA. Adaptive homeostasis and the free radical theory of ageing. *Free radical biology & medicine*. Aug 20 2018;124:420-430. doi:10.1016/j.freeradbiomed.2018.06.016
17. Stadtman ER. Protein oxidation and aging. *Science*. Aug 28 1992;257(5074):1220-4.
18. Ames BN, Shigenaga MK, Hagen TM. Oxidants, antioxidants, and the degenerative diseases of aging. *Proceedings of the National Academy of Sciences of the United States of America*. Sep 1 1993;90(17):7915-22.
19. Sohal RS, Orr WC. Relationship between antioxidants, prooxidants, and the aging process. *Annals of the New York Academy of Sciences*. Nov 21 1992;663:74-84.
20. Bokov A, Chaudhuri A, Richardson A. The role of oxidative damage and stress in aging. *Mechanisms of ageing and development*. Oct-Nov 2004;125(10-11):811-26. doi:10.1016/j.mad.2004.07.009
21. Perez VI, Bokov A, Van Remmen H, et al. Is the oxidative stress theory of aging dead? *Biochimica et biophysica acta*. Oct 2009;1790(10):1005-14. doi:10.1016/j.bbagen.2009.06.003
22. Gladyshev VN. The free radical theory of aging is dead. Long live the damage theory! *Antioxidants & redox signaling*. Feb 1 2014;20(4):727-31. doi:10.1089/ars.2013.5228
23. Hanzen S, Vielfort K, Yang J, et al. Lifespan Control by Redox-Dependent Recruitment of Chaperones to Misfolded Proteins. *Cell*. Jun 30 2016;166(1):140-51. doi:10.1016/j.cell.2016.05.006
24. Nobrega-Pereira S, Fernandez-Marcos PJ, Brioche T, et al. G6PD protects from oxidative damage and improves healthspan in mice. *Nature communications*. Mar 15 2016;7:10894. doi:10.1038/ncomms10894
25. Kubben N, Zhang W, Wang L, et al. Repression of the Antioxidant NRF2 Pathway in Premature Aging. *Cell*. Jun 2 2016;165(6):1361-1374. doi:10.1016/j.cell.2016.05.017
26. Ni J, Wu Z, Stoka V, et al. Increased expression and altered subcellular distribution of cathepsin B in microglia induce cognitive impairment through oxidative stress and inflammatory response in mice. *Aging cell*. Dec 21 2018:e12856. doi:10.1111/acel.12856
27. Sies H. Hydrogen peroxide as a central redox signaling molecule in physiological oxidative stress: Oxidative eustress. *Redox biology*. Apr 2017;11:613-619. doi:10.1016/j.redox.2016.12.035
28. Sies H, Berndt C, Jones DP. Oxidative Stress. *Annual review of biochemistry*. Jun 20 2017;86:715-748. doi:10.1146/annurev-biochem-061516-045037
29. Sohal RS, Weindruch R. Oxidative stress, caloric restriction, and aging. *Science*. Jul 5 1996;273(5271):59-63.
30. Luo H, Chiang HH, Louw M, Susanto A, Chen D. Nutrient Sensing and the Oxidative Stress Response. *Trends Endocrinol Metab*. Jun 2017;28(6):449-460. doi:10.1016/j.tem.2017.02.008

31. Qiu X, Brown KV, Moran Y, Chen D. Sirtuin regulation in calorie restriction. *Biochimica et biophysica acta*. Aug 2010;1804(8):1576-83. doi:S1570-9639(09)00263-5 [pii]
10.1016/j.bbapap.2009.09.015
32. Qiu X, Brown K, Hirschey MD, Verdin E, Chen D. Calorie Restriction Reduces Oxidative Stress by SIRT3-Mediated SOD2 Activation. *Cell metabolism*. Dec 1 2010;12(6):662-7. doi:S1550-4131(10)00407-9 [pii]
10.1016/j.cmet.2010.11.015
33. Someya S, Yu W, Hallows WC, et al. Sirt3 mediates reduction of oxidative damage and prevention of age-related hearing loss under caloric restriction. *Cell*. Nov 24 2010;143(5):802-12. doi:10.1016/j.cell.2010.10.002
34. Sundaresan NR, Gupta M, Kim G, Rajamohan SB, Isbatan A, Gupta MP. Sirt3 blocks the cardiac hypertrophic response by augmenting Foxo3a-dependent antioxidant defense mechanisms in mice. *J Clin Invest*. Sep 2009;119(9):2758-71. doi:10.1172/jci39162
35. Liu J, Li D, Zhang T, Tong Q, Ye RD, Lin L. SIRT3 protects hepatocytes from oxidative injury by enhancing ROS scavenging and mitochondrial integrity. *Cell Death Dis*. Oct 26 2017;8(10):e3158. doi:10.1038/cddis.2017.564
36. Bao J, Scott I, Lu Z, et al. SIRT3 is regulated by nutrient excess and modulates hepatic susceptibility to lipotoxicity. *Free radical biology & medicine*. Oct 15 2010;49(7):1230-7. doi:10.1016/j.freeradbiomed.2010.07.009
37. Kawamura Y, Uchijima Y, Horike N, et al. Sirt3 protects in vitro-fertilized mouse preimplantation embryos against oxidative stress-induced p53-mediated developmental arrest. *J Clin Invest*. Aug 2010;120(8):2817-28. doi:10.1172/jci42020
38. Koyama T, Kume S, Koya D, et al. SIRT3 attenuates palmitate-induced ROS production and inflammation in proximal tubular cells. *Free radical biology & medicine*. Sep 15 2011;51(6):1258-67. doi:10.1016/j.freeradbiomed.2011.05.028
39. Jing E, Emanuelli B, Hirschey MD, et al. Sirtuin-3 (Sirt3) regulates skeletal muscle metabolism and insulin signaling via altered mitochondrial oxidation and reactive oxygen species production. *Proceedings of the National Academy of Sciences of the United States of America*. Aug 30 2011;108(35):14608-13. doi:10.1073/pnas.1111308108
40. Jiang DQ, Wang Y, Li MX, Ma YJ, Wang Y. SIRT3 in Neural Stem Cells Attenuates Microglia Activation-Induced Oxidative Stress Injury Through Mitochondrial Pathway. *Frontiers in cellular neuroscience*. 2017;11:7. doi:10.3389/fncel.2017.00007
41. Xie X, Wang L, Zhao B, Chen Y, Li J. SIRT3 mediates decrease of oxidative damage and prevention of ageing in porcine fetal fibroblasts. *Life sciences*. May 15 2017;177:41-48. doi:10.1016/j.lfs.2017.01.010
42. Shi H, Deng HX, Gius D, Schumacker PT, Surmeier DJ, Ma YC. Sirt3 protects dopaminergic neurons from mitochondrial oxidative stress. *Human molecular genetics*. May 15 2017;26(10):1915-1926. doi:10.1093/hmg/ddx100
43. Zhou Y, Chung ACK, Fan R, et al. Sirt3 Deficiency Increased the Vulnerability of Pancreatic Beta Cells to Oxidative Stress-Induced Dysfunction. *Antioxidants & redox signaling*. Nov 1 2017;27(13):962-976. doi:10.1089/ars.2016.6859

44. Li Y, Yu C, Shen G, et al. Sirt3-MnSOD axis represses nicotine-induced mitochondrial oxidative stress and mtDNA damage in osteoblasts. *Acta biochimica et biophysica Sinica*. Apr 2015;47(4):306-12. doi:10.1093/abbs/gmv013
45. Winnik S, Gaul DS, Siciliani G, et al. Mild endothelial dysfunction in Sirt3 knockout mice fed a high-cholesterol diet: protective role of a novel C/EBP-beta-dependent feedback regulation of SOD2. *Basic research in cardiology*. May 2016;111(3):33. doi:10.1007/s00395-016-0552-7
46. Zhang L, Han L, Ma R, et al. Sirt3 prevents maternal obesity-associated oxidative stress and meiotic defects in mouse oocytes. *Cell cycle (Georgetown, Tex)*. 2015;14(18):2959-68. doi:10.1080/15384101.2015.1026517
47. Liu G, Cao M, Xu Y, Li Y. SIRT3 protects endothelial cells from high glucose-induced cytotoxicity. *International journal of clinical and experimental pathology*. 2015;8(1):353-60.
48. Bell EL, Emerling BM, Ricoult SJ, Guarente L. SirT3 suppresses hypoxia inducible factor 1alpha and tumor growth by inhibiting mitochondrial ROS production. *Oncogene*. Jun 30 2011;30(26):2986-96. doi:10.1038/onc.2011.37
49. Brown K, Xie S, Qiu X, et al. SIRT3 reverses aging-associated degeneration. *Cell reports*. Feb 21 2013;3(2):319-27. doi:10.1016/j.celrep.2013.01.005
50. Chen IC, Chiang WF, Liu SY, Chen PF, Chiang HC. Role of SIRT3 in the regulation of redox balance during oral carcinogenesis. *Molecular cancer*. Jun 23 2013;12:68. doi:10.1186/1476-4598-12-68
51. Jang YC, Liu Y, Hayworth CR, et al. Dietary restriction attenuates age-associated muscle atrophy by lowering oxidative stress in mice even in complete absence of CuZnSOD. *Aging cell*. Oct 2012;11(5):770-82. doi:10.1111/j.1474-9726.2012.00843.x
52. Kim HS, Patel K, Muldoon-Jacobs K, et al. SIRT3 is a mitochondria-localized tumor suppressor required for maintenance of mitochondrial integrity and metabolism during stress. *Cancer cell*. Jan 19 2010;17(1):41-52. doi:10.1016/j.ccr.2009.11.023
53. Luo H, Chiang HH, Louw M, Susanto A, Chen D. Nutrient Sensing and the Oxidative Stress Response. *Trends in endocrinology and metabolism: TEM*. Mar 14 2017;doi:10.1016/j.tem.2017.02.008
54. Shin J, Zhang D, Chen D. Reversible acetylation of metabolic enzymes celebration: SIRT2 and p300 join the party. *Molecular cell*. Jul 8 2011;43(1):3-5. doi:10.1016/j.molcel.2011.06.010
55. Traba J, Kwarteng-Siaw M, Okoli TC, et al. Fasting and refeeding differentially regulate NLRP3 inflammasome activation in human subjects. *J Clin Invest*. Nov 3 2015;125(12):4592-600. doi:10.1172/jci83260
56. Yu Y, He J, Li S, et al. Fibroblast growth factor 21 (FGF21) inhibits macrophage-mediated inflammation by activating Nrf2 and suppressing the NF-kappaB signaling pathway. *Int Immunopharmacol*. Sep 2016;38:144-52. doi:10.1016/j.intimp.2016.05.026
57. Zheng J, Shi L, Liang F, et al. Sirt3 Ameliorates Oxidative Stress and Mitochondrial Dysfunction After Intracerebral Hemorrhage in Diabetic Rats. *Frontiers in neuroscience*. 2018;12:414. doi:10.3389/fnins.2018.00414

58. Palacios OM, Carmona JJ, Michan S, et al. Diet and exercise signals regulate SIRT3 and activate AMPK and PGC-1alpha in skeletal muscle. *Aging*. Aug 15 2009;1(9):771-83. doi:10.18632/aging.100075
59. Shi T, Wang F, Stieren E, Tong Q. SIRT3, a mitochondrial sirtuin deacetylase, regulates mitochondrial function and thermogenesis in brown adipocytes. *The Journal of biological chemistry*. Apr 8 2005;280(14):13560-7. doi:10.1074/jbc.M414670200
60. Tao R, Coleman MC, Pennington JD, et al. Sirt3-mediated deacetylation of evolutionarily conserved lysine 122 regulates MnSOD activity in response to stress. *Molecular cell*. Dec 22 2010;40(6):893-904. doi:10.1016/j.molcel.2010.12.013
61. Jo SH, Son MK, Koh HJ, et al. Control of mitochondrial redox balance and cellular defense against oxidative damage by mitochondrial NADP+-dependent isocitrate dehydrogenase. *The Journal of biological chemistry*. May 11 2001;276(19):16168-76. doi:10.1074/jbc.M010120200
62. Cohen G, Hochstein P. GLUTATHIONE PEROXIDASE: THE PRIMARY AGENT FOR THE ELIMINATION OF HYDROGEN PEROXIDE IN ERYTHROCYTES. *Biochemistry*. Nov-Dec 1963;2:1420-8.
63. Esworthy RS, Ho YS, Chu FF. The Gpx1 gene encodes mitochondrial glutathione peroxidase in the mouse liver. *Archives of biochemistry and biophysics*. Apr 1 1997;340(1):59-63. doi:10.1006/abbi.1997.9901
64. Kim SC, Sprung R, Chen Y, et al. Substrate and functional diversity of lysine acetylation revealed by a proteomics survey. *Molecular cell*. Aug 2006;23(4):607-18. doi:10.1016/j.molcel.2006.06.026
65. Choudhary C, Kumar C, Gnad F, et al. Lysine acetylation targets protein complexes and co-regulates major cellular functions. *Science*. Aug 14 2009;325(5942):834-40. doi:10.1126/science.1175371
66. Zhao S, Xu W, Jiang W, et al. Regulation of cellular metabolism by protein lysine acetylation. *Science*. Feb 19 2010;327(5968):1000-4. doi:10.1126/science.1179689
67. Wegman MP, Guo MH, Bennion DM, et al. Practicality of intermittent fasting in humans and its effect on oxidative stress and genes related to aging and metabolism. *Rejuvenation research*. Apr 2015;18(2):162-72. doi:10.1089/rej.2014.1624
68. Balaban RS, Nemoto S, Finkel T. Mitochondria, oxidants, and aging. *Cell*. Feb 25 2005;120(4):483-95. doi:S0092-8674(05)00109-1 [pii]
10.1016/j.cell.2005.02.001
69. Hipp MS, Kasturi P, Hartl FU. The proteostasis network and its decline in ageing. *Nature reviews Molecular cell biology*. Feb 7 2019;doi:10.1038/s41580-019-0101-y
70. Naresh NU, Haynes CM. Signaling and Regulation of the Mitochondrial Unfolded Protein Response. *Cold Spring Harb Perspect Biol*. Jan 7 2019;doi:10.1101/cshperspect.a033944
71. Haynes CM, Ron D. The mitochondrial UPR - protecting organelle protein homeostasis. *J Cell Sci*. Nov 15 2010;123(Pt 22):3849-55. doi:10.1242/jcs.075119

72. Mohrin M, Shin J, Liu Y, et al. Stem cell aging. A mitochondrial UPR-mediated metabolic checkpoint regulates hematopoietic stem cell aging. *Science*. Mar 20 2015;347(6228):1374-7. doi:10.1126/science.aaa2361
73. Shin J, He M, Liu Y, et al. SIRT7 represses Myc activity to suppress ER stress and prevent fatty liver disease. *Cell reports*. Nov 14 2013;5(3):654-665. doi:10.1016/j.celrep.2013.10.007
74. Ryu D, Jo YS, Lo Sasso G, et al. A SIRT7-dependent acetylation switch of GABPbeta1 controls mitochondrial function. *Cell metabolism*. Nov 4 2014;20(5):856-869. doi:10.1016/j.cmet.2014.08.001
75. Fang J, Ianni A, Smolka C, et al. Sirt7 promotes adipogenesis in the mouse by inhibiting autocatalytic activation of Sirt1. *Proceedings of the National Academy of Sciences of the United States of America*. Oct 3 2017;114(40):E8352-e8361. doi:10.1073/pnas.1706945114
76. Gao M, Li X, He Y, et al. SIRT7 functions in redox homeostasis and cytoskeletal organization during oocyte maturation. *FASEB journal : official publication of the Federation of American Societies for Experimental Biology*. Jun 7 2018:fj201800078RR. doi:10.1096/fj.201800078RR
77. Yan WW, Liang YL, Zhang QX, et al. Arginine methylation of SIRT7 couples glucose sensing with mitochondria biogenesis. *EMBO reports*. Dec 2018;19(12)doi:10.15252/embr.201846377
78. Lopez-Otin C, Blasco MA, Partridge L, Serrano M, Kroemer G. The hallmarks of aging. *Cell*. Jun 6 2013;153(6):1194-217. doi:10.1016/j.cell.2013.05.039
79. Partridge L, Deelen J, Slagboom PE. Facing up to the global challenges of ageing. *Nature*. Sep 2018;561(7721):45-56. doi:10.1038/s41586-018-0457-8
80. Chen J, Astle CM, Harrison DE. Hematopoietic senescence is postponed and hematopoietic stem cell function is enhanced by dietary restriction. *Experimental hematology*. Nov 2003;31(11):1097-103.
81. Ertl RP, Chen J, Astle CM, Duffy TM, Harrison DE. Effects of dietary restriction on hematopoietic stem-cell aging are genetically regulated. *Blood*. Feb 1 2008;111(3):1709-16. doi:10.1182/blood-2007-01-069807
82. Yilmaz OH, Katajisto P, Lamming DW, et al. mTORC1 in the Paneth cell niche couples intestinal stem-cell function to calorie intake. *Nature*. Jun 28 2012;486(7404):490-5. doi:10.1038/nature11163
83. Cerletti M, Jang YC, Finley LW, Haigis MC, Wagers AJ. Short-term calorie restriction enhances skeletal muscle stem cell function. *Cell Stem Cell*. May 4 2012;10(5):515-9. doi:10.1016/j.stem.2012.04.002
84. Park JH, Glass Z, Sayed K, et al. Calorie restriction alleviates the age-related decrease in neural progenitor cell division in the aging brain. *The European journal of neuroscience*. Jun 2013;37(12):1987-93. doi:10.1111/ejn.12249
85. Folmes CD, Dzeja PP, Nelson TJ, Terzic A. Metabolic plasticity in stem cell homeostasis and differentiation. *Cell Stem Cell*. Nov 2 2012;11(5):596-606. doi:10.1016/j.stem.2012.10.002
86. Takubo K, Goda N, Yamada W, et al. Regulation of the HIF-1alpha level is essential for hematopoietic stem cells. *Cell Stem Cell*. Sep 3 2010;7(3):391-402. doi:10.1016/j.stem.2010.06.020

87. Takubo K, Nagamatsu G, Kobayashi CI, et al. Regulation of glycolysis by Pdk functions as a metabolic checkpoint for cell cycle quiescence in hematopoietic stem cells. *Cell Stem Cell*. Jan 3 2013;12(1):49-61. doi:10.1016/j.stem.2012.10.011
88. Naka K, Hoshii T, Muraguchi T, et al. TGF-beta-FOXO signalling maintains leukaemia-initiating cells in chronic myeloid leukaemia. *Nature*. Feb 4 2010;463(7281):676-80. doi:10.1038/nature08734
89. Kops GJ, Dansen TB, Polderman PE, et al. Forkhead transcription factor FOXO3a protects quiescent cells from oxidative stress. *Nature*. Sep 19 2002;419(6904):316-21. doi:10.1038/nature01036
90. Mohrin M, Chen D. The mitochondrial metabolic checkpoint and aging of hematopoietic stem cells. *Curr Opin Hematol*. Jul 2016;23(4):318-24. doi:10.1097/moh.0000000000000244
91. Juntilla MM, Patil VD, Calamito M, Joshi RP, Birnbaum MJ, Koretzky GA. AKT1 and AKT2 maintain hematopoietic stem cell function by regulating reactive oxygen species. *Blood*. May 20 2010;115(20):4030-8. doi:10.1182/blood-2009-09-241000
92. Chen C, Liu Y, Liu R, et al. TSC-mTOR maintains quiescence and function of hematopoietic stem cells by repressing mitochondrial biogenesis and reactive oxygen species. *J Exp Med*. Sep 29 2008;205(10):2397-408. doi:10.1084/jem.20081297
93. Ito K, Hirao A, Arai F, et al. Regulation of oxidative stress by ATM is required for self-renewal of haematopoietic stem cells. *Nature*. Oct 21 2004;431(7011):997-1002. doi:10.1038/nature02989
94. Maryanovich M, Oberkovitz G, Niv H, et al. The ATM-BID pathway regulates quiescence and survival of haematopoietic stem cells. *Nature cell biology*. Mar 25 2012;14(5):535-41. doi:10.1038/ncb2468
95. Miyamoto K, Araki KY, Naka K, et al. Foxo3a is essential for maintenance of the hematopoietic stem cell pool. *Cell Stem Cell*. Jun 7 2007;1(1):101-12. doi:10.1016/j.stem.2007.02.001
96. Tothova Z, Kollipara R, Huntly BJ, et al. FoxOs are critical mediators of hematopoietic stem cell resistance to physiologic oxidative stress. *Cell*. Jan 26 2007;128(2):325-39. doi:10.1016/j.cell.2007.01.003
97. Tsai JJ, Dudakov JA, Takahashi K, et al. Nrf2 regulates haematopoietic stem cell function. *Nature cell biology*. Mar 2013;15(3):309-16. doi:10.1038/ncb2699
98. Jung H, Kim MJ, Kim DO, et al. TXNIP maintains the hematopoietic cell pool by switching the function of p53 under oxidative stress. *Cell metabolism*. Jul 2 2013;18(1):75-85. doi:10.1016/j.cmet.2013.06.002
99. Mohrin M, Widjaja A, Liu Y, Luo H, Chen D. The mitochondrial unfolded protein response is activated upon hematopoietic stem cell exit from quiescence. *Aging cell*. Jun 2018;17(3):e12756. doi:10.1111/acel.12756
100. Owusu-Ansah E, Banerjee U. Reactive oxygen species prime Drosophila haematopoietic progenitors for differentiation. *Nature*. Sep 24 2009;461(7263):537-41. doi:10.1038/nature08313
101. Ito K, Hirao A, Arai F, et al. Reactive oxygen species act through p38 MAPK to limit the lifespan of hematopoietic stem cells. *Nature medicine*. Apr 2006;12(4):446-51. doi:10.1038/nm1388

102. Luo H, Mu WC, Karki R, et al. Mitochondrial Stress-Initiated Aberrant Activation of the NLRP3 Inflammasome Regulates the Functional Deterioration of Hematopoietic Stem Cell Aging. *Cell Rep*. Jan 22 2019;26(4):945-954.e4. doi:10.1016/j.celrep.2018.12.101
103. Nakahira K, Haspel JA, Rathinam VA, et al. Autophagy proteins regulate innate immune responses by inhibiting the release of mitochondrial DNA mediated by the NALP3 inflammasome. *Nat Immunol*. Mar 2011;12(3):222-30. doi:10.1038/ni.1980
104. Grant RW, Dixit VD. Mechanisms of disease: inflammasome activation and the development of type 2 diabetes. *Front Immunol*. 2013;4:50. doi:10.3389/fimmu.2013.00050
105. Guo H, Callaway JB, Ting JP. Inflammasomes: mechanism of action, role in disease, and therapeutics. *Nature medicine*. Jul 2015;21(7):677-87. doi:10.1038/nm.3893
106. Misawa T, Takahama M, Kozaki T, et al. Microtubule-driven spatial arrangement of mitochondria promotes activation of the NLRP3 inflammasome. *Nat Immunol*. May 2013;14(5):454-60. doi:10.1038/ni.2550
107. Paik JH, Ding Z, Narurkar R, et al. FoxOs cooperatively regulate diverse pathways governing neural stem cell homeostasis. *Cell Stem Cell*. Nov 6 2009;5(5):540-53. doi:10.1016/j.stem.2009.09.013
108. Renault VM, Rafalski VA, Morgan AA, et al. FoxO3 regulates neural stem cell homeostasis. *Cell Stem Cell*. Nov 6 2009;5(5):527-39. doi:10.1016/j.stem.2009.09.014
109. Webb AE, Pollina EA, Vierbuchen T, et al. FOXO3 shares common targets with ASCL1 genome-wide and inhibits ASCL1-dependent neurogenesis. *Cell reports*. Aug 15 2013;4(3):477-91. doi:10.1016/j.celrep.2013.06.035
110. Yeo H, Lyssiotis CA, Zhang Y, et al. FoxO3 coordinates metabolic pathways to maintain redox balance in neural stem cells. *The EMBO journal*. Oct 2 2013;32(19):2589-602. doi:10.1038/emboj.2013.186
111. Hochmuth CE, Biteau B, Bohmann D, Jasper H. Redox regulation by Keap1 and Nrf2 controls intestinal stem cell proliferation in Drosophila. *Cell Stem Cell*. Feb 4 2011;8(2):188-99. doi:10.1016/j.stem.2010.12.006
112. Wang XQ, Shao Y, Ma CY, et al. Decreased SIRT3 in aged human mesenchymal stromal/stem cells increases cellular susceptibility to oxidative stress. *Journal of cellular and molecular medicine*. Nov 2014;18(11):2298-310. doi:10.1111/jcmm.12395
113. Zhang H, Ryu D, Wu Y, et al. NAD(+) repletion improves mitochondrial and stem cell function and enhances life span in mice. *Science*. Jun 17 2016;352(6292):1436-43. doi:10.1126/science.aaf2693
114. Berger E, Rath E, Yuan D, et al. Mitochondrial function controls intestinal epithelial stemness and proliferation. *Nature communications*. Oct 27 2016;7:13171. doi:10.1038/ncomms13171
115. Gertz M, Steegborn C. Using mitochondrial sirtuins as drug targets: disease implications and available compounds. *Cellular and molecular life sciences : CMLS*. Aug 2016;73(15):2871-96. doi:10.1007/s00018-016-2180-7

116. Yang Y, Sauve AA. NAD(+) metabolism: Bioenergetics, signaling and manipulation for therapy. *Biochimica et biophysica acta*. Dec 2016;1864(12):1787-1800. doi:10.1016/j.bbapap.2016.06.014
117. Bieganowski P, Brenner C. Discoveries of nicotinamide riboside as a nutrient and conserved NRK genes establish a Preiss-Handler independent route to NAD+ in fungi and humans. *Cell*. May 14 2004;117(4):495-502.
118. Bender DA. Biochemistry of tryptophan in health and disease. *Molecular aspects of medicine*. 1983;6(2):101-97.
119. Canto C, Menzies KJ, Auwerx J. NAD(+) Metabolism and the Control of Energy Homeostasis: A Balancing Act between Mitochondria and the Nucleus. *Cell metabolism*. Jul 7 2015;22(1):31-53. doi:10.1016/j.cmet.2015.05.023
120. Yoshino J, Mills KF, Yoon MJ, Imai S. Nicotinamide mononucleotide, a key NAD(+) intermediate, treats the pathophysiology of diet- and age-induced diabetes in mice. *Cell metabolism*. Oct 5 2011;14(4):528-36. doi:10.1016/j.cmet.2011.08.014
121. Mouchiroud L, Houtkooper RH, Moullan N, et al. The NAD(+)/Sirtuin Pathway Modulates Longevity through Activation of Mitochondrial UPR and FOXO Signaling. *Cell*. Jul 18 2013;154(2):430-41. doi:10.1016/j.cell.2013.06.016
122. Stein LR, Imai S. Specific ablation of Nampt in adult neural stem cells recapitulates their functional defects during aging. *The EMBO journal*. Jun 17 2014;33(12):1321-40. doi:10.1002/embj.201386917
123. Gomes AP, Price NL, Ling AJ, et al. Declining NAD(+) induces a pseudohypoxic state disrupting nuclear-mitochondrial communication during aging. *Cell*. Dec 19 2013;155(7):1624-38. doi:10.1016/j.cell.2013.11.037
124. Yoshino M, Yoshino J, Kayser BD, et al. Nicotinamide mononucleotide increases muscle insulin sensitivity in prediabetic women. *Science*. Jun 11 2021;372(6547):1224-1229. doi:10.1126/science.abe9985
125. Katsyuba E, Mottis A, Zietak M, et al. De novo NAD(+) synthesis enhances mitochondrial function and improves health. *Nature*. Nov 2018;563(7731):354-359. doi:10.1038/s41586-018-0645-6
126. Canto C, Houtkooper RH, Pirinen E, et al. The NAD(+) precursor nicotinamide riboside enhances oxidative metabolism and protects against high-fat diet-induced obesity. *Cell metabolism*. Jun 6 2012;15(6):838-47. doi:10.1016/j.cmet.2012.04.022
127. Brown KD, Maqsood S, Huang JY, et al. Activation of SIRT3 by the NAD(+) precursor nicotinamide riboside protects from noise-induced hearing loss. *Cell metabolism*. Dec 2 2014;20(6):1059-68. doi:10.1016/j.cmet.2014.11.003
128. Vannini N, Campos V, Girotra M, et al. The NAD-Booster Nicotinamide Riboside Potently Stimulates Hematopoiesis through Increased Mitochondrial Clearance. *Cell Stem Cell*. Mar 7 2019;24(3):405-418.e7. doi:10.1016/j.stem.2019.02.012
129. Martens CR, Denman BA, Mazzo MR, et al. Chronic nicotinamide riboside supplementation is well-tolerated and elevates NAD(+) in healthy middle-aged and older adults. *Nature communications*. Mar 29 2018;9(1):1286. doi:10.1038/s41467-018-03421-7
130. Pillai VB, Samant S, Sundaresan NR, et al. Honokiol blocks and reverses cardiac hypertrophy in mice by activating mitochondrial Sirt3. *Nature communications*. Apr 14 2015;6:6656. doi:10.1038/ncomms7656

131. Ramesh S, Govindarajulu M, Lynd T, et al. SIRT3 activator Honokiol attenuates beta-Amyloid by modulating amyloidogenic pathway. *PloS one*. 2018;13(1):e0190350. doi:10.1371/journal.pone.0190350
132. Ye JS, Chen L, Lu YY, Lei SQ, Peng M, Xia ZY. SIRT3 activator honokiol ameliorates surgery/anesthesia-induced cognitive decline in mice through anti-oxidative stress and anti-inflammatory in hippocampus. *CNS neuroscience & therapeutics*. Sep 17 2018;doi:10.1111/cns.13053
133. Sheu ML, Chiang CK, Tsai KS, et al. Inhibition of NADPH oxidase-related oxidative stress-triggered signaling by honokiol suppresses high glucose-induced human endothelial cell apoptosis. *Free radical biology & medicine*. Jun 15 2008;44(12):2043-50. doi:10.1016/j.freeradbiomed.2008.03.014
134. Rauf A, Olatunde A, Imran M, et al. Honokiol: A review of its pharmacological potential and therapeutic insights. *Phytomedicine*. Sep 2021;90:153647. doi:10.1016/j.phymed.2021.153647
135. Lu J, Zhang H, Chen X, et al. A small molecule activator of SIRT3 promotes deacetylation and activation of manganese superoxide dismutase. *Free radical biology & medicine*. Nov 2017;112:287-297. doi:10.1016/j.freeradbiomed.2017.07.012
136. Hor JH, Santosa MM, Lim VJW, et al. ALS motor neurons exhibit hallmark metabolic defects that are rescued by SIRT3 activation. *Cell Death Differ*. Apr 2021;28(4):1379-1397. doi:10.1038/s41418-020-00664-0
137. Coll RC, Robertson AA, Chae JJ, et al. A small-molecule inhibitor of the NLRP3 inflammasome for the treatment of inflammatory diseases. *Nature medicine*. Mar 2015;21(3):248-55. doi:10.1038/nm.3806
138. Xu KY, Wu CY, Tong S, Xiong P, Wang SH. The selective Nlrp3 inflammasome inhibitor Mcc950 attenuates lung ischemia-reperfusion injury. *Biochemical and biophysical research communications*. Sep 18 2018;503(4):3031-3037. doi:10.1016/j.bbrc.2018.08.089
139. Bartke A. Minireview: role of the growth hormone/insulin-like growth factor system in mammalian aging. *Endocrinology*. Sep 2005;146(9):3718-23. doi:10.1210/en.2005-0411
140. Fontana L, Partridge L, Longo VD. Extending healthy life span--from yeast to humans. *Science*. Apr 16 2010;328(5976):321-6. doi:10.1126/science.1172539
141. Garinis GA, Uittenboogaard LM, Stachelscheid H, et al. Persistent transcription-blocking DNA lesions trigger somatic growth attenuation associated with longevity. *Nature cell biology*. May 2009;11(5):604-15. doi:10.1038/ncb1866
142. Kanfi Y, Naiman S, Amir G, et al. The sirtuin SIRT6 regulates lifespan in male mice. *Nature*. Feb 22 2012;483(7388):218-21. doi:10.1038/nature10815
143. Kenyon C. The plasticity of aging: insights from long-lived mutants. *Cell*. Feb 25 2005;120(4):449-60. doi:10.1016/j.cell.2005.02.002
144. Murphy CT, McCarroll SA, Bargmann CI, et al. Genes that act downstream of DAF-16 to influence the lifespan of Caenorhabditis elegans. *Nature*. Jul 17 2003;424(6946):277-83. doi:10.1038/nature01789
145. Niedernhofer LJ, Garinis GA, Raams A, et al. A new progeroid syndrome reveals that genotoxic stress suppresses the somatotroph axis. *Nature*. Dec 21 2006;444(7122):1038-43. doi:10.1038/nature05456

146. Vermeij WP, Dolle ME, Reiling E, et al. Restricted diet delays accelerated ageing and genomic stress in DNA-repair-deficient mice. *Nature*. Sep 15 2016;537(7620):427-431. doi:10.1038/nature19329
147. Weindruch RaW, R.L. *The retardation of aging and disease by dietary restriction.* 1988.
148. Chishima S, Kogiso T, Matsushita N, Hashimoto E, Tokushige K. The Relationship between the Growth Hormone/Insulin-like Growth Factor System and the Histological Features of Nonalcoholic Fatty Liver Disease. *Internal medicine (Tokyo, Japan)*. 2017;56(5):473-480. doi:10.2169/internalmedicine.56.7626
149. Colak Y, Senates E, Ozturk O, et al. Serum concentrations of human insulin-like growth factor-1 and levels of insulin-like growth factor-binding protein-5 in patients with nonalcoholic fatty liver disease: association with liver histology. *Eur J Gastroenterol Hepatol*. Mar 2012;24(3):255-61. doi:10.1097/MEG.0b013e32834e8041
150. Dal K, Bulur O, Ata N, et al. The role of insulin - like growth factor - 1 on steatohepatitis. *Acta Gastroenterol Belg*. Jan-Mar 2017;80(1):21-24.
151. Dichtel LE, Corey KE, Misdraji J, et al. The Association Between IGF-1 Levels and the Histologic Severity of Nonalcoholic Fatty Liver Disease. *Clin Transl Gastroenterol*. Jan 26 2017;8(1):e217. doi:10.1038/ctg.2016.72
152. Fusco A, Miele L, D'Uonnolo A, et al. Nonalcoholic fatty liver disease is associated with increased GHBP and reduced GH/IGF-I levels. *Clinical endocrinology*. Oct 2012;77(4):531-6. doi:10.1111/j.1365-2265.2011.04291.x
153. Garcia-Galiano D, Sanchez-Garrido MA, Espejo I, et al. IL-6 and IGF-1 are independent prognostic factors of liver steatosis and non-alcoholic steatohepatitis in morbidly obese patients. *Obes Surg*. Apr 2007;17(4):493-503. doi:10.1007/s11695-007-9087-1
154. Hribal ML, Procopio T, Petta S, et al. Insulin-like growth factor-I, inflammatory proteins, and fibrosis in subjects with nonalcoholic fatty liver disease. *The Journal of clinical endocrinology and metabolism*. Feb 2013;98(2):E304-8. doi:10.1210/jc.2012-3290
155. Liang S, Cheng X, Hu Y, Song R, Li G. Insulin-like growth factor 1 and metabolic parameters are associated with nonalcoholic fatty liver disease in obese children and adolescents. *Acta Paediatr*. Feb 2017;106(2):298-303. doi:10.1111/apa.13685
156. Liang S, Yu Z, Song X, Wang Y, Li M, Xue J. Reduced Growth Hormone Secretion is Associated with Nonalcoholic Fatty Liver Disease in Obese Children. *Hormone and metabolic research = Hormon- und Stoffwechselforschung = Hormones et metabolisme*. Mar 2018;50(3):250-256. doi:10.1055/s-0043-124970
157. Mallea-Gil MS, Ballarino MC, Spiraquis A, et al. IGF-1 levels in different stages of liver steatosis and its association with metabolic syndrome. *Acta Gastroenterol Latinoam*. Mar 2012;42(1):20-6.
158. Cohen JC, Horton JD, Hobbs HH. Human fatty liver disease: old questions and new insights. *Science*. Jun 24 2011;332(6037):1519-23. doi:10.1126/science.1204265

159. Kim JY, Garcia-Carbonell R, Yamachika S, et al. ER Stress Drives Lipogenesis and Steatohepatitis via Caspase-2 Activation of S1P. *Cell*. Sep 20 2018;175(1):133-145 e15. doi:10.1016/j.cell.2018.08.020
160. Wang M, Kaufman RJ. Protein misfolding in the endoplasmic reticulum as a conduit to human disease. *Nature*. Jan 21 2016;529(7586):326-35. doi:10.1038/nature17041
161. Costa-Mattioli M, Walter P. The integrated stress response: From mechanism to disease. *Science*. Apr 24 2020;368(6489)doi:10.1126/science.aat5314
162. Jones JI, Clemmons DR. Insulin-like growth factors and their binding proteins: biological actions. *Endocrine reviews*. Feb 1995;16(1):3-34. doi:10.1210/edrv-16-1-3
163. Xia W, Wang Y, Zhang Y, et al. Endoplasmic reticulum stress induces growth retardation by inhibiting growth hormone IGF-I axis. *Growth Horm IGF Res*. Dec 2020;55:101341. doi:10.1016/j.ghir.2020.101341
164. Vazquez BN, Thackray JK, Simonet NG, et al. SIRT7 promotes genome integrity and modulates non-homologous end joining DNA repair. *The EMBO journal*. Jul 15 2016;35(14):1488-503. doi:10.15252/embj.201593499
165. Walter P, Ron D. The unfolded protein response: from stress pathway to homeostatic regulation. *Science*. Nov 25 2011;334(6059):1081-6. doi:10.1126/science.1209038
166. Jiang HY, Wek SA, McGrath BC, et al. Activating transcription factor 3 is integral to the eukaryotic initiation factor 2 kinase stress response. *Mol Cell Biol*. Feb 2004;24(3):1365-77. doi:10.1128/mcb.24.3.1365-1377.2004
167. Rouillard AD, Gundersen GW, Fernandez NF, et al. The harmonizome: a collection of processed datasets gathered to serve and mine knowledge about genes and proteins. *Database (Oxford)*. 2016;2016doi:10.1093/database/baw100
168. Mayr B, Montminy M. Transcriptional regulation by the phosphorylation-dependent factor CREB. *Nature reviews Molecular cell biology*. Aug 2001;2(8):599-609. doi:10.1038/35085068
169. Kim JY, Park KJ, Hwang JY, et al. Activating transcription factor 3 is a target molecule linking hepatic steatosis to impaired glucose homeostasis. *J Hepatol*. Aug 2017;67(2):349-359. doi:10.1016/j.jhep.2017.03.023
170. Zhao P, Saltiel AR. From Overnutrition to Liver Injury: AMP-Activated Protein Kinase in Nonalcoholic Fatty Liver Diseases. *The Journal of biological chemistry*. Jul 10 2020;doi:10.1074/jbc.REV120.011356
171. Zhao P, Sun X, Chaggan C, et al. An AMPK-caspase-6 axis controls liver damage in nonalcoholic steatohepatitis. *Science*. Feb 7 2020;367(6478):652-660. doi:10.1126/science.aay0542
172. Dorn C, Engelmann JC, Saugspier M, et al. Increased expression of c-Jun in nonalcoholic fatty liver disease. *Lab Invest*. Apr 2014;94(4):394-408. doi:10.1038/labinvest.2014.3
173. Vansaun MN, Mendonsa AM, Lee Gorden D. Hepatocellular proliferation correlates with inflammatory cell and cytokine changes in a murine model of nonalchoholic fatty liver disease. *PloS one*. 2013;8(9):e73054. doi:10.1371/journal.pone.0073054

174. Zhu C, Tabas I, Schwabe RF, Pajvani UB. Maladaptive regeneration - the reawakening of developmental pathways in NASH and fibrosis. *Nat Rev Gastroenterol Hepatol*. Feb 2021;18(2):131-142. doi:10.1038/s41575-020-00365-6
175. Zhu Q, Wang H, Jiang B, et al. Loss of ATF3 exacerbates liver damage through the activation of mTOR/p70S6K/ HIF-1alpha signaling pathway in liver inflammatory injury. *Cell Death Dis*. Sep 5 2018;9(9):910. doi:10.1038/s41419-018-0894-1
176. Cabrera D, Ruiz A, Cabello-Verrugio C, et al. Diet-Induced Nonalcoholic Fatty Liver Disease Is Associated with Sarcopenia and Decreased Serum Insulin-Like Growth Factor-1. *Dig Dis Sci*. Nov 2016;61(11):3190-3198. doi:10.1007/s10620-016-4285-0
177. Farrell GC, Larter CZ, Hou JY, et al. Apoptosis in experimental NASH is associated with p53 activation and TRAIL receptor expression. *J Gastroenterol Hepatol*. Mar 2009;24(3):443-52. doi:10.1111/j.1440-1746.2009.05785.x
178. Guarino M, Kumar P, Felser A, et al. Exercise Attenuates the Transition from Fatty Liver to Steatohepatitis and Reduces Tumor Formation in Mice. *Cancers (Basel)*. May 29 2020;12(6)doi:10.3390/cancers12061407
179. Katsyuba E, Romani M, Hofer D, Auwerx J. NAD(+) homeostasis in health and disease. *Nat Metab*. Jan 2020;2(1):9-31. doi:10.1038/s42255-019-0161-5
180. Montllor-Albalate C, Song Z, Chen D. The therapeutic promises of NAD(+) boosters. *Cell metabolism*. Jul 6 2021;33(7):1274-1275. doi:10.1016/j.cmet.2021.06.008
181. Rajman L, Chwalek K, Sinclair DA. Therapeutic Potential of NAD-Boosting Molecules: The In Vivo Evidence. *Cell metabolism*. Mar 6 2018;27(3):529-547. doi:10.1016/j.cmet.2018.02.011
182. Tarrago MG, Chini CCS, Kanamori KS, et al. A Potent and Specific CD38 Inhibitor Ameliorates Age-Related Metabolic Dysfunction by Reversing Tissue NAD(+) Decline. *Cell metabolism*. May 1 2018;27(5):1081-1095 e10. doi:10.1016/j.cmet.2018.03.016
183. Drew L. Fighting the fatty liver. *Nature*. Oct 11 2017;550(7675):S102-S103. doi:10.1038/550S102a
184. Loomba R, Friedman SL, Shulman GI. Mechanisms and disease consequences of nonalcoholic fatty liver disease. *Cell*. May 13 2021;184(10):2537-2564. doi:10.1016/j.cell.2021.04.015
185. Perry RJ, Samuel VT, Petersen KF, Shulman GI. The role of hepatic lipids in hepatic insulin resistance and type 2 diabetes. *Nature*. Jun 5 2014;510(7503):84-91. doi:10.1038/nature13478
186. Woo Baidal JA, Lavine JE. The intersection of nonalcoholic fatty liver disease and obesity. *Sci Transl Med*. Jan 27 2016;8(323):323rv1. doi:10.1126/scitranslmed.aad8390
187. Chen D, Steele AD, Lindquist S, Guarente L. Increase in activity during calorie restriction requires Sirt1. *Science*. Dec 9 2005;310(5754):1641. doi:10.1126/science.1118357

188. Cohen HY, Miller C, Bitterman KJ, et al. Calorie restriction promotes mammalian cell survival by inducing the SIRT1 deacetylase. *Science*. Jul 16 2004;305(5682):390-2. doi:10.1126/science.1099196
189. Wu T, Liu YH, Fu YC, Liu XM, Zhou XH. Direct evidence of sirtuin downregulation in the liver of non-alcoholic fatty liver disease patients. *Ann Clin Lab Sci*. Fall 2014;44(4):410-8.
190. Xu X, Deng X, Chen Y, Xu W, Xu F, Liang H. SIRT1 mediates nutritional regulation of SREBP-1c-driven hepatic PNPLA3 transcription via modulation of H3k9 acetylation. *Genes Environ*. May 27 2022;44(1):18. doi:10.1186/s41021-022-00246-1
191. Dahl TB, Haukeland JW, Yndestad A, et al. Intracellular nicotinamide phosphoribosyltransferase protects against hepatocyte apoptosis and is down-regulated in nonalcoholic fatty liver disease. *The Journal of clinical endocrinology and metabolism*. Jun 2010;95(6):3039-47. doi:10.1210/jc.2009-2148
192. Parker R, Schmidt MS, Cain O, Gunson B, Brenner C. Nicotinamide Adenine Dinucleotide Metabolome Is Functionally Depressed in Patients Undergoing Liver Transplantation for Alcohol-Related Liver Disease. *Hepatol Commun*. Aug 2020;4(8):1183-1192. doi:10.1002/hep4.1530
193. Luo H, Mu WC, Karki R, et al. Mitochondrial Stress-Initiated Aberrant Activation of the NLRP3 Inflammasome Regulates the Functional Deterioration of Hematopoietic Stem Cell Aging. *Cell Rep*. Jan 22 2019;26(4):945-954 e4. doi:10.1016/j.celrep.2018.12.101
194. Dahl JA, Collas P. A quick and quantitative chromatin immunoprecipitation assay for small cell samples. *Front Biosci*. 2007;12:4925-31.
195. Tabula Muris C, Overall c, Logistical c, et al. Single-cell transcriptomics of 20 mouse organs creates a Tabula Muris. *Nature*. Oct 2018;562(7727):367-372. doi:10.1038/s41586-018-0590-4
196. Gonçalves LA, Vigário AM, Penha-Gonçalves C. Improved isolation of murine hepatocytes for in vitro malaria liver stage studies. *Malar J*. 2007;6:169-169. doi:10.1186/1475-2875-6-169
197. Hoh CH, Tan YH, Gan YH. Protective Role of Kupffer Cells and Macrophages in Klebsiella pneumoniae-Induced Liver Abscess Disease. *Infection and immunity*. Sep 2019;87(9)doi:10.1128/iai.00369-19
198. Wolf FA, Angerer P, Theis FJ. SCANPY: large-scale single-cell gene expression data analysis. *Genome Biol*. Feb 6 2018;19(1):15. doi:10.1186/s13059-017-1382-0
199. Traag VA, Waltman L, van Eck NJ. From Louvain to Leiden: guaranteeing well-connected communities. *Scientific reports*. Mar 26 2019;9(1):5233. doi:10.1038/s41598-019-41695-z
200. Finak G, McDavid A, Yajima M, et al. MAST: a flexible statistical framework for assessing transcriptional changes and characterizing heterogeneity in single-cell RNA sequencing data. *Genome Biol*. Dec 10 2015;16:278. doi:10.1186/s13059-015-0844-5
201. Zadravec D, Brolinson A, Fisher RM, et al. Ablation of the very-long-chain fatty acid elongase ELOVL3 in mice leads to constrained lipid storage and resistance to diet-induced obesity. *FASEB journal : official publication of the Federation of*

American Societies for Experimental Biology. Nov 2010;24(11):4366-77. doi:10.1096/fj.09-152298
202. Schneider CA, Rasband WS, Eliceiri KW. NIH Image to ImageJ: 25 years of image analysis. *Nat Methods*. Jul 2012;9(7):671-5. doi:10.1038/nmeth.2089